

# Emergent stability in complex network dynamics

Chandrakala Meena,<sup>1–3</sup> Chittaranjan Hens,<sup>4</sup> Suman Acharyya,<sup>1,2</sup> Simcha Haber,<sup>1</sup>

Stefano Boccaletti<sup>5–8</sup> & Baruch Barzel<sup>1,2,\*</sup>

1. Department of Mathematics, Bar-Ilan University, Ramat-Gan, Israel
2. Gonda Multidisciplinary Brain Research Center, Bar-Ilan University, Ramat-Gan, Israel
3. Chemical Engineering and Process Development, CSIR-National Chemical Laboratory, Pune 411008, Maharashtra, India
4. Physics and Applied Mathematics Unit, Indian Statistical Institute, Kolkata, India
5. CNR - Institute of Complex Systems, Via Madonna del Piano 10, Sesto Fiorentino I-50019, Italy
6. Unmanned Systems Research Institute, Northwestern Polytechnical University, Xi'an 710072, China
7. Moscow Institute of Physics and Technology (National Research University), 9 Institutskiy per., Dolgoprudny, Moscow Region 141701, Russian Federation
8. Universidad Rey Juan Carlos, Calle Tulipán s/n, 28933 Móstoles, Madrid, Spain

\* Correspondence: baruchbarzel@gmail.com

*In memory of Prof. Robert May*

The stable functionality of networked systems is a hallmark of their natural ability to coordinate between their multiple interacting components. Yet, strikingly, real-world networks seem random and highly irregular, apparently lacking any design for stability. What then are the naturally emerging organizing principles of complex-system stability? Encoded within the system's stability matrix, the Jacobian, the answer is obscured by the scale and diversity of the relevant systems, their broad parameter space, and their nonlinear interaction mechanisms. To make advances, here we uncover emergent patterns in the structure of the Jacobian, rooted in the interplay between the network topology and the system's intrinsic nonlinear dynamics. These patterns help us analytically identify the few relevant control parameters that determine a system's dynamic stability. Complex systems, we find, exhibit discrete stability classes, from asymptotically unstable, where stability is unattainable, to sensitive, in which stability abides within a bounded range of the system's parameters. Most crucially, alongside these two classes, we uncover a third class, asymptotically stable, in which a sufficiently large and heterogeneous network acquires a guaranteed stability, independent of parameters, and therefore insensitive to external perturbation. Hence, two of the most ubiquitous characteristics of real-world networks - scale and heterogeneity - emerge as natural organizing principles to ensure stability in the face of changing environmental conditions.

The study of complex social, biological and technological systems, is often directed towards dramatic events, such as cascading failures<sup>1–5</sup> or abrupt state transitions.<sup>6–10</sup> In reality, however, these represent the exception rather than the rule. In fact, the truly intriguing phenomenon is that, despite enduring constant perturbations and local obstructions, many systems continue to sustain reliably stable dynamics.<sup>11–14</sup> This is achieved in the absence of a detailed design, as indeed, the dynamics of the majority of complex systems are mediated by random, often extremely heterogeneous, networks, comprising a large number of interacting components, and driven by a vast space of microscopic parameters. What then are the roots of the observed stability?

To address this we seek the system's linear stability matrix, namely its Jacobian  $J$ , whose principal eigenvalue  $\lambda$  determines its response to perturbation.<sup>15,16</sup> According to linear stability theory, perturbations may either grow exponentially ( $\text{Re}(\lambda) > 0$ ), capturing instability, or decay exponentially ( $\text{Re}(\lambda) < 0$ ), if the system is at a stable state. These distinct behaviors depend on the detailed structure of  $J$ , and therefore predicting complex system stability boils down to two crucial challenges:

**Theoretical.** The first challenge is of mathematical nature - how do we uncover the structure of  $J$ , given the scale, diversity and multiple parameters characterizing real-world complex systems? Indeed, for low-dimensional systems, with just few interacting components,  $J$  can be calculated explicitly around each of the system's potential states. However, such explicit construction becomes intractable as the number of components  $N$  is increased, making it difficult to predict the system's stability.<sup>17</sup> The common paradigm is to bypass this difficulty by extracting  $J$  from the random matrix ensemble, allowing a simple construction, with well-established spectral properties.<sup>18,19</sup> However, this approach, we show, overlooks emergent patterns in  $J$ , rooted in the system's dynamic mechanisms, that have profound impact on stability.

**Practical.** Regardless of our ability to calculate  $J$ , it remains unclear how real systems calibrate their structural/dynamic parameters to ensure that this  $J$  is stable. Indeed, random matrix theory indicates that, unless specifically designed for stability, a random  $J$  is extremely unlikely to have  $\text{Re}(\lambda) < 0$ . We, therefore, seek to uncover naturally emerging organizing principles that secure stability without having to *fine-tune* the system's vast number of microscopic parameters.

Here, we address both challenges by extracting the structure of real-world Jacobian matrices directly from the system's intrinsic nonlinear dynamics. We discover a new, non-random, Jacobian ensemble, in which topology and dynamics are deeply intertwined. Under this ensemble, stability is determined by a small set of analytically attainable parameters that capture the combined contribution of both topology *and* dynamics. Most crucially, the ensemble includes a broad class of frequently encountered dynamic mechanisms, for which stability becomes *inevitable* in the limit of  $N \rightarrow \infty$ . Such systems exhibit an *emergent stability*, that becomes asymptotically independent of microscopic parameters, offering a natural design principle to ensure complex system stability.<sup>20-22</sup>

## Fixed-point dynamics

Consider a complex system of  $N$  interacting components (nodes), whose dynamic activities  $\mathbf{x}(t) = (x_1(t), \dots, x_N(t))^\top$  are driven by nonlinear pairwise interactions. The system's fixed-points  $\mathbf{x}_\alpha$  capture static states, which, unperturbed, remain independent of time. The dynamics in the vicinity of these fixed-point can be examined through the system's response to small perturbations  $\delta\mathbf{x}(t)$ , which, in the linear regime, can be approximated by

$$\frac{d\delta\mathbf{x}}{dt} = J\delta\mathbf{x} + O(\delta\mathbf{x}^2). \quad (1)$$

Here  $J$ , an  $N \times N$  matrix, represents the system's Jacobian around  $\mathbf{x}_\alpha$ , which approximates, through a set of linear equations, the original nonlinear system's dynamics in the perturbative limit, *i.e.* small activity changes  $\mathbf{x}(t) = \mathbf{x}_\alpha + \delta\mathbf{x}(t)$ . Hence,  $J$ 's spectral properties, and specifically its principal eigenvalue  $\lambda$ , are of crucial importance in characterizing the system's fixed-point behavior.

Two factors shape the Jacobian - the system's topology, *i.e.* its patterns of interaction, and its

internal dynamics, capturing the mechanisms of these interactions:

**Topology.** The first ingredient that impacts the structure of  $J$  is the network topology  $A$ , a binary matrix ( $A_{ij} \in \{0, 1\}$ ,  $A_{ii} = 0$ ), which is typically sparse and, most often, highly heterogeneous.<sup>23</sup> As  $J$  is designed to capture the *direct* response between  $i$  and  $j$ , its off-diagonal terms vanish in case there is no direct  $i, j$  link, *i.e.*  $A_{ij} = 0 \iff J_{ij} = 0$  for all  $i \neq j$ . If, however  $A_{ij} = 1$ , then the relevant term is assigned a *weight*  $J_{ij} = W_{ij}$  that captures the strength of the  $i, j$  linear dependence. Together, this leads to

$$J = (A - I) \otimes W, \quad (2)$$

where the Hadamard product  $\otimes$  represents matrix multiplication element by element, and  $I$  is the  $N \times N$  identity matrix. In (2) the network structure ( $A$ ) determines the non-vanishing off-diagonal terms in  $J$ , and  $W$  determined their weights. The diagonal entries  $J_{ii}$  are introduced through the second term in (2),  $I \otimes W$ , where  $W_{ii}$  quantifies  $x_i(t)$ 's self-linear dependence.

**The random matrix paradigm.** To complete the construction of (2) we must assign all weights  $W$ . In many of the traditional analyses these unknown weights are extracted from two pre-selected distributions,  $P_0(w)$  and  $P_1(w)$ , capturing the probability density functions of the diagonal ( $P_0$ ) and off-diagonal ( $P_1$ ) weights. This gives rise to the Jacobian ensemble  $\mathbb{E}(A, P_0, P_1)$ , in which one first constructs the topology  $A$ , then assigns diagonal and off-diagonal weights from  $P_0(w)$  and  $P_1(w)$ , respectively (Fig. 1a-c).

As a classic example for this ensemble, we consider May's<sup>18</sup> construction, in which  $A$  is an Erdős-Rényi (ER) network, the off-diagonal weights are extracted via  $W_{ij} \sim \mathcal{N}(0, \sigma^2)$ , a zero-mean normal distribution, and the diagonal entries are taken uniformly as  $W_{ii} = 1$ . This captures the fact that the interaction strengths are potentially random, hence the distributed nature of  $W_{ij}$ , while the self-dynamics are driven by the system's intrinsic relaxation time-scales, as expressed by the fixed value of all  $W_{ii}$ , here set to unity.

More generally, one can consider more complex  $A_{ij}$ , *e.g.*, sparse or scale-free,<sup>19</sup> which have, indeed, been shown to impact (2)'s spectral properties. Similarly, the weight distributions may also be generalized, allowing distributed time-scales via  $P_0(w)$ , or diverse, often scale-free, interaction strengths, through a fat-tailed  $P_1(w)$ .

Despite its simplicity, the  $\mathbb{E}(A, P_0, P_1)$  ensemble has two crucial shortcomings: (i) it provides no explicit guidelines to connect  $P_0(w)$  and  $P_1(w)$  with the system's specific nonlinear interaction mechanisms; (ii) by assigning  $A$  and  $W$  independently, it ignores the potential interplay between the network structure and  $J$ 's dynamic weights. Consequently, in  $\mathbb{E}(A, P_0, P_1)$  if two systems share a similar topology  $A$ , they will have an equally similar  $J$  (up to statistical variations), regardless of their dynamics, social, biological or technological. This, of course, stands in sharp contrast with the frequently observed fact that different nonlinear mechanisms, despite being supported by the same network, may express fundamentally distinct dynamic behaviors.<sup>24-26</sup>

In reality, one expects  $J$  not only to distinguish between different types of dynamics, but even between different fixed-points within the *same* dynamics. Indeed, if a system has two fixed-points, a stable  $\mathbf{x}_\alpha$  and a non-stable  $\mathbf{x}_\beta$ , they must each be characterized by a different  $J$  matrix, a stable  $J$  around  $\mathbf{x}_\alpha$  and an unstable one around  $\mathbf{x}_\beta$ . Such distinctions are absent in the random matrix paradigm underlying the  $\mathbb{E}(A, P_0, P_1)$  ensemble.

How then do we appropriately assign the weights  $W$  in (2) to capture the role of the system's

dynamics? For low dimensional systems of few components, this can be done on a case by case basis, by explicitly calculating all linear dependencies. However, for complex, often highly heterogeneous networks, in which not only is  $N \gg 1$ , but all individual nodes are also potentially diverse, we lack a systematic construction of  $J$ , limiting our ability to predict complex system fixed-point dynamics. We, therefore, now seek the general rules that govern the structure of  $J$ , *i.e.* the relevant  $J$ -ensemble for real-world network dynamics.

## The dynamic Jacobian ensemble

**Dynamic mechanisms** (Fig. 1d). To construct realistic  $J$  matrices we consider each system's specific nonlinear dynamic mechanisms. For example, in epidemic dynamics, individuals interact through infection and recovery,<sup>27–29</sup> in biological networks, proteins, genes and metabolites are linked through biochemical processes<sup>30–33</sup> and in population dynamics, species undergo competitive or symbiotic interactions.<sup>34–37</sup> Most generally, these dynamic mechanisms can be described by<sup>24</sup>

$$\frac{dx_i}{dt} = M_0(x_i(t), \mathbf{f}_i) + \mathcal{G} \sum_{j=1}^N A_{ij} M_1(x_i(t)) G_{ij} M_2(x_j(t)), \quad (3)$$

where  $M_0(x_i, \mathbf{f}_i)$  captures the self-dynamics of all nodes, and the product function  $M_1(x_i)M_2(x_j)$  describes the  $i, j$  pairwise interaction. With the appropriate selection of these three nonlinear functions  $\mathbf{M} = (M_0(x), M_1(x), M_2(x))$ , Eq. (3) captures a broad range of frequently used models in social,<sup>27,28</sup> biological<sup>30–34</sup> and technological<sup>38</sup> systems (Fig. 2). The dynamics in (3) incorporate a set of tunable parameters: the self-dynamics of each node is characterized by the parameter set  $\mathbf{f}_i$ , and the global interaction rate between all nodes is controlled by  $\mathcal{G}$ , whose value increases/decreases the strength of *all* interactions. Besides that, the specific interaction strength between  $i$  and  $j$  is governed by the network weights  $G_{ij}$ , allowing potentially diverse link weights.

Equation (3) goes beyond topology  $A$ , introducing also the dynamics. It therefore allows us to capture the role of the nonlinearity and its impact on  $J$ . Before we use it to extract  $J$ , however, we wish to distinguish between the role of its different components • **Dynamic mechanisms** (Fig. 1e). The functions  $M_0, M_1, M_2$  in  $\mathbf{M}$  describe the system's intrinsic mechanisms, ingrained into the natural processes driving its interacting units. Indeed, the functional form of  $\mathbf{M}$  distinguishes between, *e.g.*, social vs. biological dynamics, capturing built-in mechanisms that are hardwired into the *physics* of the system components. These functions are therefore fixed and uniform across all nodes/links, *i.e.* they are *intrinsic*. • **Parameters** (Fig. 1f,g).  $\mathbf{f} = (f_1, \dots, f_N)$  and  $G_{ij}$ , in contrast, capture the node/link specific parameters, which may be potentially diverse, depending on the particular rates characterizing each node or the unique strength of each interaction. Similarly, the global weight  $\mathcal{G}$ , is also subject to the effect of external conditions, which may increase/decrease the typical interaction rates. Hence,  $f, \mathcal{G}$  and  $G$  are *non-intrinsic*.

To understand this distinction let us consider a specific example of epidemic spreading via the susceptible-infected-susceptible (SIS) dynamics, *i.e.* Epidemic in Fig. 2a. First, we focus on the self-dynamics  $M_0(x_i, \mathbf{f}_i) = -f_i x_i$ . This function describes the process of recovery, in which an infected node ( $\mathcal{I}$ ) transitions to the susceptible state ( $\mathcal{S}$ ) at a rate  $f_i$ , *i.e.*  $\mathcal{I} \xrightarrow{f_i} \mathcal{S}$ . Such transition is captured by a *linear* function  $M_0(x_i) \propto x_i$ , whose slope represents its single *rate* parameter  $f_i$ . The crucial point is, that while the rate  $f_i$  is idiosyncratic and changes from one individual to another, the *linear form* of  $M_0$  is intrinsic to the nature of the recovery process, and is therefore,

uniform across all nodes. Hence  $M_0$ 's functional form is fixed (*dynamic mechanism*. Fig. 1e), while its rate constant  $f_i$  is tunable (*parameter*, Fig. 1f).

Similarly, the nonlinear interactions of Epidemic,  $M_1(x_i)G_{ij}M_2(x_j) = (1-x_i)G_{ij}x_j$ , are universal across all linked pairs - embedded in the nature of the SIS infection mechanism  $\mathcal{I} + \mathcal{S} \xrightarrow{G_{ij}} 2\mathcal{I}$ . This is while the rates  $G_{ij}$  depend on the unique strength of the  $i, j$  social tie, or on  $i$  and  $j$ 's individual propensity for contracting the disease. Therefore, in (3) the *functional form* of  $\mathbf{M}$  is fixed, representing the *built-in physical* mechanisms that drive all nodes/links, while the *parameters*  $\mathbf{f}, \mathcal{G}, G$  are potentially diverse and/or tunable due to external conditions.

Below we seek patterns in  $J$  that can be traced to the nonlinear Eq. (3), distinguishing, along the lines of the above discussion, between the contribution of (i) the intrinsic nonlinear mechanisms  $\mathbf{M}$ ; (ii) the potentially diverse parameters  $\mathbf{f}, \mathcal{G}, G$  and (iii) the network topology  $A$ .

**Real-world Jacobians** (Fig. 1h). To obtain realistic  $J$  matrices we relinquish the random matrix construction  $\mathbb{E}(A, P_0, P_1)$ , and extract the Jacobian directly from (3), hence incorporating not just the network structure  $A$ , but also the system's nonlinear dynamics  $\mathbf{M}$ . In Supplementary Section 1, we show that this leads to a currently unexplored matrix ensemble, in which the Jacobian weights  $W$  in (2) are strongly intertwined with the weighted topology  $A, G$  via

$$W_{ii} \sim C(\mathbf{f}, \mathcal{G}) \mathcal{D}_{nn}^\eta d_i^\mu \quad (4)$$

for the diagonal weights  $J_{ii} = -W_{ii}$ , and

$$W_{ij} \sim d_i^\nu G_{ij} d_j^\rho \quad (5)$$

for the off-diagonal weights  $J_{ij} = A_{ij}W_{ij}$  ( $i \neq j$ ).

In (4) and (5)  $d_i = \sum_{j=1}^N A_{ij}G_{ij}$  represents the weighted degree of node  $i$ , and

$$\mathcal{D}_{nn} = \frac{1}{N} \sum_{i=1}^N \frac{1}{d_i} \sum_{j=1}^N A_{ij}G_{ij}d_j \quad (6)$$

represents the average weighted degree of a nearest neighbor node.<sup>7</sup> The coefficient  $C = C(\mathbf{f}, \mathcal{G})$  is governed by the system's specific parameters  $\mathbf{f} = (\mathbf{f}_1, \dots, \mathbf{f}_N)^\top$  and  $\mathcal{G}$ , which, as noted above, are *non-intrinsic*. Finally, the four exponents,  $\Omega = (\eta, \mu, \nu, \rho)$  are fully determined by the system's *intrinsic* dynamic mechanisms,  $\mathbf{M}$ , as shown in **Appendix I**.

The resulting dynamic  $J$  in (4) and (5) is fundamentally distinct from the existing random matrix based constructions. On the one hand, the network structure  $A$  continues to determine the non-zero entries, similarly to the classic ensemble  $\mathbb{E}(A, P_0, P_1)$ . Also, the typical magnitude of the diagonal entries is determined by the system's rates constants through  $\mathbf{f}$  and  $\mathcal{G}$ , once again, analogous, albeit not identical, to the selection of  $P_0(w)$  in the existing ensemble. However, the similarity ends there, as (4) and (5), in contrast to  $\mathbb{E}(A, P_0, P_1)$ , also capture the role of the *intrinsic nonlinear mechanisms*. Indeed, they predict emergent patterns in the structure of real-world Jacobian matrices, that are rooted in the interplay between topology and dynamics: The degrees  $\mathcal{D}_{nn}, d_i$  are extracted from the *weighted network topology*  $A \otimes G$  ((Fig. 1g), while the scaling exponents  $\Omega$  are derived from the *nonlinear dynamics*  $\mathbf{M}$  (Fig. 1e). Therefore, we arrive at a new Jacobian ensemble  $\mathbb{E}(A, G, \Omega)$ , which, unlike the random matrix based treatment of  $\mathbb{E}(A, P_0, P_1)$ , accounts for the effect of the system-specific nonlinear mechanisms. Consequently,

in  $\mathbb{E}(A, G, \Omega)$ , identical networks may give rise to highly distinctive Jacobian matrices, depending on whether the interactions are, *e.g.*, social, biological or ecological, as each of these mechanisms is characterized by its unique set of exponents  $\Omega$ , and, consequently, its unique fixed-point dynamics (Fig. 1h).

**Testing  $\mathbb{E}(A, G, \Omega)$ .** To examine predictions (4) and (5) we constructed a broad testing ground, on which we implemented seven relevant dynamic models from social, biological and technological domains: *Epidemic*. The SIS model<sup>27–29</sup> for disease spreading • *Regulatory*. The Michaelis-Menten model<sup>30</sup> for gene regulation • *Inhibitory*. Growth suppression in pathogen-host interactions<sup>36</sup> • *Biochemical*. Protein-protein interactions<sup>31–33</sup> in sub-cellular networks • *Population 1,2*. Mutualistic<sup>34</sup> interactions in population dynamics • *Power*. Load distribution in electric transmission networks. Applying each of these dynamics to five different model and relevant empirical networks, we arrive at a total of 35 combinations of networks/dynamics, upon which we test our predicted  $J$ -ensemble (for a detailed description of all dynamic models and networks see Supplementary Sections 3 and 4).

In Fig. 2 we present, for each system, its dynamic equation (blue), and list the relevant networks upon which it was tested (violet). In some cases the system features several fixed-points, for example, Epidemic (Fig. 2a) exhibits a healthy state (inactive  $\mathbf{x}_0$ ) and a pandemic state (active  $\mathbf{x}_1$ ). These states are presented using a 3D visualization. The network is laid out on the  $x, y$  plane, and the activity  $x_i$  of all nodes is captured by the vertical  $z$ -axis displacement. Hence under  $\mathbf{x}_0$  all nodes remain on the  $x, y$  plane ( $z = 0$ ), while in the active  $\mathbf{x}_1$  they all have  $x_i > 0$ . Finally, we derive the dynamic exponents  $\Omega = (\eta, \mu, \nu, \rho)$  for each system around its active state (orange); see Supplementary Section 3, where we also treat the inactive states.

Perturbing the system around its active fixed-point, we constructed the Jacobian matrix  $J$  for each of our 35 systems. In Fig. 3 we find that, indeed, the diagonal ( $W_{ii}$ ) and off-diagonal ( $W_{ij}$ ) weights of  $J$  follow the predicted scaling of (4) and (5). For example, in Epidemic we predict  $\mu = 1$ , while for Regulatory we have  $\mu = 0$ , both scaling relationships clearly evident in Fig. 3b and d. This means that extracting all diagonal terms independently from  $P_0(w)$ , as in  $\mathbb{E}(A, P_0, P_1)$ , misses the actual patterns that arise from the nonlinear Epidemic/Regulatory dynamics. Similarly, the off-diagonal terms are proportional to  $d_i^{-1}G_{ij}d_j^0$  in Epidemic (Fig. 3c) and  $d_i^0G_{ij}d_j^{-2}$  in Regulatory (Fig. 3e), once again overruling the random construction in which  $W_{ij}$  are extracted from an arbitrary  $P_1(w)$ .

Our analysis further predicts that these scaling relationships, encapsulated within our analytically predicted  $\Omega$ , are intrinsic to the nonlinear dynamics  $\mathbf{M}$ , thus independent of the network structure  $A$  or the specific parameters  $\mathbf{f}, \mathcal{G}$  and  $G$ . We examine this in Fig. 3, by testing each of our dynamics on a diverse set of networks, with different degree/weight distributions. As predicted, we find that  $\eta, \mu, \nu$  and  $\rho$  are, indeed, universal, conserved across our distinct model (Erdős-Rényi, Scale-free 1, Scale-free 2) and relevant empirical (Social 1,2, PPI 1,2, etc.) networks. Hence,  $\Omega$  captures the intrinsic, and most crucially, hitherto overlooked, contribution of the nonlinear *dynamics* to the structure of  $J$ .

Together, our derivation demonstrates that: (i) actual  $J$  matrices, extracted from real nonlinear dynamics are fundamentally distinct from the commonly used random ensembles; (ii) contrary to the random  $J$  ensembles, real Jacobians feature non-random scaling patterns in which topology ( $\mathcal{D}_{nn}, d_i$ ) and dynamics ( $\Omega$ ) are deeply intertwined; (iii) these patterns can be analytically traced to the system's intrinsic nonlinear mechanisms ( $\mathbf{M}$ ) through Eqs. (4) and (5), giving rise to our new ensemble  $\mathbb{E}(A, G, \Omega)$ . Next, we use  $\mathbb{E}(A, G, \Omega)$  to derive the conditions for Eq. (3)'s dynamic

stability.

## Topology, dynamics and the emergence of stability

The dynamic stability of (3) around a given fixed-point is governed by  $J$ 's principal eigenvalue  $\lambda$ , requiring that  $\text{Re}(\lambda) < 0$ . We, therefore, seek the contribution of the weighted topology  $(A, G$ , Fig. 1g), the system specific parameters  $(\mathbf{f}, \mathcal{G}$ , Fig. 1f) and its nonlinear dynamic mechanisms  $(\mathbf{M}$ , Fig. 1e) to the value of  $\text{Re}(\lambda)$ .

First, let us focus on the weighted topology. The ingredients of  $J \in \mathbb{E}(A, G, \Omega)$ , as expressed in Eqs. (4) and (5), suggest that  $\lambda$  is strongly linked to the network's weighted degree distribution  $P(d)$ . This is indicated directly through the dependence on  $d_i$  and  $d_j$ , but also indirectly through the nearest neighbor degree  $\mathcal{D}_{\text{nn}}$ , whose magnitude depends on the system's degree-heterogeneity.<sup>39</sup> For instance, in a random network with uniform weights we have  $\mathcal{D}_{\text{nn}} = \langle d^2 \rangle / \langle d \rangle$ ,<sup>7,19</sup> in which the second moment  $\langle d^2 \rangle$  increases with  $P(d)$ 's variance, and consequently with  $A$ 's heterogeneity. Most generally, for a fat-tailed  $P(d)$ , we have<sup>39</sup>

$$\mathcal{D}_{\text{nn}} \sim N^\beta, \quad (7)$$

an asymptotic divergence with system size. Hence,  $\beta$  is driven by the network heterogeneity, being  $\beta = 0$  for homogeneous networks, in which  $P(d)$  is bounded, and  $\beta > 0$  for heterogeneous  $A, G$ , where  $P(d)$  is fat-tailed.

The second ingredient which impacts  $\lambda$  in  $\mathbb{E}(A, G, \Omega)$  is  $\Omega = (\eta, \mu, \nu, \rho)$ , designed to capture the role of the dynamics  $\mathbf{M}$ . Finally,  $C(\mathbf{f}, \mathcal{G})$ , the pre-factor in the scaling relationship of (4), encapsulates the contribution of the non-intrinsic, potentially tunable, parameters. Combining all three contributions together, we show in Supplementary Section 2 that in  $\mathbb{E}(A, G, \Omega)$ , the principal eigenvalue asymptotically follows

$$\text{Re}(\lambda) \sim N^Q \left( 1 - \frac{C}{N^S} \right), \quad (8)$$

where  $Q = \beta(1 + \nu + \rho - \eta/2)$  and

$$S = \beta(\mathbf{s} + \nu + \rho - \mu - \eta). \quad (9)$$

In (9), the parameter  $\mathbf{s}$  depends on the *sign* of the interactions, being  $\mathbf{s} = 1$  under cooperative interactions (positive  $J_{ij}$ ), such as in Epidemic or Regulatory, and  $\mathbf{s} = 0$  if the interactions are adversarial (negative  $J_{ij}$ ), *e.g.* Inhibitory or Biochemical.

Equations (8)-(9), our key result, uncover the asymptotic behavior of  $\lambda$  in the limit of a large complex system  $N \rightarrow \infty$ . Contrary to  $\mathbb{E}(A, P_0, P_1)$ , in which  $\lambda$  is fully determined by  $A$  and  $G$ , here the exponents  $S$  and  $Q$  capture the interplay of structure *and* dynamics, via  $\Omega$ . Most importantly, these equations have crucial implications regarding the system's fixed-point stability, giving rise to three potential stability classes (Fig. 1i):

- **Asymptotic instability** ( $S > 0$ , red). In case  $S$  in (8) is positive, we have, for sufficiently large  $N$ ,  $\text{Re}(\lambda) \sim N^Q > 0$ . This asymptotic behavior is independent of  $C$ , which represents the only term in (8) that depends on  $\mathbf{f}, \mathcal{G}$ . Therefore, such fixed-points, in a large enough system, become intrinsically unstable, regardless of the model parameters.

- **Asymptotic stability** ( $S < 0$ , blue). For  $S < 0$  we have  $N^S \rightarrow 0$ , the r.h.s. of (8) is dominated by the negative term, and hence  $\text{Re}(\lambda) < 0$ , independently of  $C$ . Hence, here in the limit  $N \rightarrow \infty$ , stability becomes unconditionally guaranteed, once again unaffected by the system's specific parameters  $\mathbf{f}, \mathcal{G}$ .
- **Sensitive stability** ( $S = 0$ , green). Under  $S = 0$  the system lacks an asymptotic behavior, and therefore, its stability depends on  $C$  in (8). If  $C > 1$  the system is stable, otherwise it becomes unstable. Consequently, in this class stability is not an intrinsic characteristic of the *system*. Rather it is driven by Eq. (3)'s specific tunable parameters.

**Stability classifier.** The *stability classifier*  $S$  in (9) helps group all  $J \in \mathbb{E}(A, G, \Omega)$  into distinct stability classes. It achieves this by identifying the relevant topological ( $\beta$ ) and dynamic ( $\Omega$ ) control parameters that help analytically predict the stability of any system within the form (3). We can therefore use  $S$  to predict *a priori* whether a specific combination of topology and dynamics will exhibit stable functionality or not.

To examine  $S$ 's predictive power we used our model and real networks to extract 7,387 Jacobian matrices from the  $\mathbb{E}(A, G, \Omega)$  ensemble, with different sets of  $\eta, \mu, \nu$  and  $\rho$ . In Fig. 4a we show the principal eigenvalue  $\lambda$  vs.  $S$  for the entire 7,387 Jacobian sample. As predicted, we find that the parameter  $S$  sharply splits the sample into three classes. The asymptotically unstable class (red, top-right) has  $S > 0$  and consequently also  $\lambda > 0$ , a guaranteed instability. The asymptotically stable class (blue, bottom-left) is observed for  $S < 0$ , and has, in all cases  $\lambda < 0$ , *i.e.* stable dynamics. Finally, for  $S = 0$  we observe sensitive stability, with  $\lambda$  having no asymptotic positive/negative assignment (green). A small fraction ( $\sim 8\%$ ) of our sampled  $J$  matrices were inaccurately classified by  $S$  (grey), a consequence of the approximate nature of our derivations (Supplementary Section 2).

Figures 3 and 4, together, demonstrate our theoretical path up to this point: First, Fig. 3 shows that real  $J$  matrices exhibit the internal scaling patterns predicted in (4) and (5) - representing a steep departure from the broadly applied random matrix paradigm of  $\mathbb{E}(A, P_0, P_1)$ . Next, Fig. 4 shows that the resulting Jacobian ensemble  $\mathbb{E}(A, G, \Omega)$  has a rich stability profile, profoundly distinct from the currently considered  $\mathbb{E}(A, P_0, P_1)$ , and, most importantly, fully characterized by a single parameter - our analytically predicted classifier  $S$ . We can now use  $S$  to analyze the structural and dynamic ingredients that contribute to complex system stability.

## The ingredients of dynamic stability

The parameter  $S$  in (9) reduces a network's dynamic stability into five relevant exponents. The first four  $\Omega = (\eta, \mu, \nu, \rho)$  are determined by the nonlinear dynamics  $\mathbf{M}$ , Epidemic, Regulatory, Population etc., and are therefore intrinsic to the system's inherent interaction mechanisms. These exponents are independent of the topology  $A$ , its weights  $G$ , or of the microscopic model parameters  $\mathbf{f}$  and  $\mathcal{G}$ . Therefore they are *hardwired* into the system's dynamic behavior.

The remaining exponent in (9),  $\beta$ , is independent of the dynamics, determined solely by  $A, G$ , specifically by the weighted degree distribution  $P(d)$ , through (7). Therefore, together,  $S$  captures the roles of both topology *and* dynamics, whose interplay determines the system's stability class around a specific fixed-point - stable, unstable or sensitive.

**The role of degree-heterogeneity.** The prevalence of fat-tailed  $P(d)$  is among the defining features of real-world complex systems, from biological<sup>40</sup> to social<sup>41,42</sup> and technological<sup>43,44</sup> networks, with far-reaching implications on their observed dynamic behavior.<sup>7,19,24</sup> Our analysis

indicates that this universal network characteristic may also play a crucial role in the context of dynamic stability.

To understand this, consider a bounded  $P(d)$ , such as an ER network with uniform weights. Here the weighted degrees follow a Poisson distribution, having  $\beta = 0$ . Under these conditions we have  $S = 0$  in (9), the system has no defined asymptotic behavior, and hence it is sensitively stable - *i.e.* its stability depends on model parameters via  $C$ . Therefore, our predicted asymptotically stable/unstable classes, which depend on  $\beta > 0$ , are, in fact, a direct consequence of degree-heterogeneity.

This uncovers a new, previously overlooked, layer to the dynamic impact of  $P(d)$  on complex system functionality. Consider, for example, the factors that drive a system towards the loss of stability. Most often such events result from external stress or changes in environmental conditions.<sup>7</sup> Such forces impact the system by perturbing its dynamic parameters, namely they affect the coefficient  $C$ . Seldom, however, do these environmental perturbations affect the system's built-in interaction mechanisms. Indeed, as discussed above, these mechanisms are ingrained in the *physics* of the interacting components, therefore unaffected by external conditions. The crucial point is, that under  $S < 0$ , a state only possible if  $P(d)$  is fat-tailed, stability becomes asymptotically independent of  $C$ , driven solely by  $\Omega$ , which is insensitive to the non-intrinsic model parameters. Hence, for a sufficiently large system ( $N \rightarrow \infty$ ), if  $P(d)$  is fat-tailed, stability becomes asymptotically robust against any external perturbation. *This suggests that degree/weight-heterogeneity serves as a dynamically stabilizing topological characteristics, in the face of a persistently fluctuating environment.*

#### BOX I. Solving a 50 year old puzzle

Will a large complex system be stable? This question, first posed by May in 1972,<sup>18</sup> captures a long standing challenge, fueled by the seeming contradiction between theory and practice. While empirical reality answers with an astounding yes, May's mathematical analysis, based on random matrix theory, suggests the contrary, giving rise to the *diversity-stability paradox*. What, then, are the organizing principles, or in May's original wording - *nature's devious strategies*, that enable complex system stability.

Initial clues began to unveil with the mapping of empirical networks, which uncovered universally recurring topological characteristics<sup>23,45</sup> that can potentially impact the system's dynamics.<sup>17</sup> For example, degree heterogeneity,<sup>46</sup> community structure<sup>39</sup> or topological symmetries<sup>47-49</sup> - all naturally emerging features of real-world networks - were suggested as potentially stabilizing structures. In ecology, constraints on populations sizes offered additional paths to stability.<sup>21,22</sup>

Our framework settles this dichotomy, quite naturally, by departing from the prevailing random matrix paradigm, captured via  $\mathbb{E}(A, P_0, P_1)$ , in favor of our analytically derived  $\mathbb{E}(A, G, \Omega)$ . In this new  $J$ -ensemble, the system's intrinsic dynamic mechanisms lead to the emergence of built-in scaling patterns in  $J$ , that are absent in the random matrix framework. These patterns, in turn, predict a broad class of *asymptotically stable dynamics*, in which May's original question receives a clear answer: large complex systems not only *can*, but, often *must* be stable.

**Will a large complex system be stable?** To gain deeper insight into roots of asymptotic stability/instability, we consider again  $\mathbb{E}(A, G, \Omega)$ 's principal eigenvalue  $\lambda$  in (8). Its structure portrays stability as a balance between the positive, *i.e.* destabilizing, effect mediated by the network interactions, vs. the negative, stabilizing, feedback, driven by the parameter  $C$  in  $J$ 's

diagonal (4); Fig. 4b. It is therefore, natural to enhance stability by increasing  $C$ , which, in effect, translates to strengthening each node's intrinsic negative feedback. Equation (8) predicts that  $J$  becomes stable if  $C$  exceeds a critical value

$$C_0 \sim N^S, \quad (10)$$

beyond which  $\lambda$  becomes negative. For asymptotically stable systems ( $S < 0$ ) we have, for sufficiently large  $N$ ,  $C_0 \rightarrow 0$ , a guaranteed stability even under arbitrarily small  $C$ . In contrast, for asymptotically unstable systems ( $S > 0$ ) we have  $C_0 \rightarrow \infty$ , hence such systems are impossible to stabilize even under extremely large  $C$ . We emphasize that  $C = C(\mathbf{f}, \mathcal{G})$  is the only component in (8) that is dependent on the system's tunable parameters, and therefore having an unbounded range of  $C$  values under which the system remains stable (or unstable) guarantees that  $\lambda$  is unaffected by parameter perturbation, *e.g.*, changing environmental conditions.

To test Eq. (10) in Fig. 4c-k we extract a set of three specific  $J$  matrices from  $\mathbb{E}(A, G, \Omega)$ , representing systems from our three stability classes:  $J_{\text{AS}}$ , asymptotically stable with  $\Omega = (2, 2, 2, -1)$ ;  $J_{\text{SS}}$ , sensitively stable with  $\Omega = (0, -1, -2, 0)$ ; and  $J_{\text{AU}}$ , asymptotically unstable with  $\Omega = (1, -2, -1, 2)$ . For each of these we plot  $C_0$  vs.  $N$ , capturing the level of negative feedback required to ensure the system's stability. Under ER ( $\beta = 0$ ) we do not observe a defined asymptotic behavior. The critical  $C_0$  does not scale with  $N$ , indicating that sufficient perturbation to the model parameters can, indeed, affect the system's stability (Fig. 4i-k, green circles).

Constructing the same  $J$  matrices from our scale-free network SF1 ( $\beta = 0.6$ ), we now observe a clear asymptotic behavior, congruent with prediction (10). For  $J_{\text{AS}}$  we have  $C_0 \sim N^{-1.2}$ , while under  $J_{\text{AU}}$  we observe  $C_0 \sim N^{1.8}$  (Fig. 4f-h), capturing the intrinsic stability/instability of these two systems. Finally, in  $J_{\text{SS}}$ , having  $S = 0$ , the system, again lacks an asymptotic behavior, and therefore can be stabilized under finite  $C_0$ , independently of system size  $N$  (Fig. 4g). Together, Eq. (10) helps us link the scale  $N$  of a complex system with its observed stability. As opposed to the random matrix viewpoint of  $\mathbb{E}(A, P_0, P_1)$ , in which  $N$  has a *destabilizing* effect,<sup>18</sup> our dynamic ensemble uncovers broad conditions where the contrary is true, and  $N \rightarrow \infty$ , is, in fact, what anchors the system's stability (**Box I**).

**Emergent stability.** This observation on the stabilizing/destabilizing effect of  $N$  and  $P(d)$  is especially relevant if (3) exhibits multiple fixed-points, for example, an undesirable  $\mathbf{x}_0$  and a desirable  $\mathbf{x}_1$ . For a low-dimensional system ( $N$  small) transitions between these points are controlled by the system *parameters*. This is also the case if the system is large ( $N \rightarrow \infty$ ) but homogeneous ( $\beta = 0$ ). Indeed, both cases belong to the sensitively stable class ( $S = 0$ ), in which  $\lambda$  in (8) shows no asymptotic trend - either due to the finite value of  $N$  or due to the fact that  $\beta = 0$ . Such parameter-driven state transitions capture the classic view of dynamic stability: the potential fixed-points are rooted in the system's intrinsic nonlinear dynamics, their stability, on the other hand, is determined by its specific, and most crucially, tunable parameters.<sup>7</sup>

The picture, however, changes fundamentally when the network is large and heterogeneous, *i.e.*  $N \rightarrow \infty$  and  $\beta > 0$ . This is because in  $\mathbb{E}(A, G, \Omega)$  each of the system's fixed-points may be potentially characterized by a unique set of dynamic exponents,  $\mathbf{x}_0$ 's Jacobian having the set  $\Omega_0$  and  $\mathbf{x}_1$  having  $\Omega_1$  (Fig. 5a,b). If, for instance,  $\Omega_0$  has  $S > 0$  in (9) and  $\Omega_1$  has  $S < 0$ , then  $\mathbf{x}_0$  becomes asymptotically *unstable* and  $\mathbf{x}_1$  becomes asymptotically *stable*. Such systems will be guaranteed to reside only in  $\mathbf{x}_1$ , unaffected by perturbation to their parameters.

To observe this we return to our testing ground of Fig. 2, this time focusing on dynamic models

that have multiple fixed-points. This includes Regulatory, Epidemic and Inhibitory, each of which exhibits on top of its *active* state  $\mathbf{x}_1$ , in which all  $x_i > 0$ , an *inactive* state  $\mathbf{x}_0 = (0, \dots, 0)^\top$ , where all activities vanish (Population 1,2 also exhibit an inactive  $\mathbf{x}_0$ , however it is never stable, see Supplementary Section 3.3).

First, we simulated Regulatory 1 ( $a = h = 1$ ) on an ER network, and varied the model's two parameters  $\mathbf{f}, \mathcal{G}$ . We find that when the average  $\langle \mathbf{f} \rangle$  is large or, alternatively, when  $\mathcal{G}$  is small the system resides in  $\mathbf{x}_0$ , whereas in the opposite limit, it favors  $\mathbf{x}_1$  (Fig. 5c-e, diamonds). This is precisely the *sensitive stability*, in which the system's fixed-point behavior is driven by its tunable parameters. Repeating the same experiment on our scale-free network SF1, we observe that  $\mathbf{x}_1$  is sustained for a broader range of  $\langle \mathbf{f} \rangle$  and  $\mathcal{G}$ , hence SF1 is comparably insensitive to these parameters (Fig. 5d-f, triangles). This robustness is a direct outcome of our classifier:  $\mathbf{x}_0$  has  $\Omega_0 = (0, 0, 0, 0)$ , which in (9) predicts  $S = \beta > 0$ , while  $\mathbf{x}_1$  has  $\Omega_1 = (0, 1, 0, -2)$ , and hence  $S = -\beta < 0$ . Therefore, on a large scale-free network  $\mathbf{x}_0$  becomes asymptotically unstable, and the system is forced to reside in the asymptotically stable  $\mathbf{x}_1$ .

To observe this systematically we seek the critical global weight  $\mathcal{G}_c$ , below which  $\mathbf{x}_1$  becomes unstable, and the system transitions to  $\mathbf{x}_0$ . Varying the system size  $N$  over  $\sim 4$  orders of magnitude, we observe first hand  $\mathbf{x}_1$ 's asymptotic stability: while under ER  $\mathcal{G}_c$  is almost independent of  $N$  (Fig. 5g, diamonds), in SF1 it scales negatively with system size, approaching  $\mathcal{G}_c \rightarrow 0$  in the limit  $N \rightarrow \infty$  (triangles). Hence, as predicted SF1 remains stable even under arbitrarily small  $\mathcal{G}_c$ . This reconfirms prediction (10), but this time, not on theoretically constructed  $J$  from  $\mathbb{E}(A, G, \Omega)$ , as shown in Fig. 4f-k, but rather on the actual numerically calculated dynamics of Eq. (3). Similar stability patterns are also observed in Epidemic and Inhibitory (Fig. 5h,i and Supplementary Sections 3.1 and 3.5).

*Hence, we observe a qualitative difference between bounded vs. scale-free  $P(d)$ , in which degree-heterogeneity can potentially afford the network a guaranteed stability, that is asymptotically independent of microscopic parameters.*

**Equivalence classes of dynamic stability.** While stability is, in its essence, a binary classification - a fixed-point is either stable or not, we can use  $S$  to quantify the *level* of the system's stability around a given fixed-point. Consider again  $C_0$  in (10), capturing the critical value of  $C$  in (4) required to stabilize the system's dynamics. For large  $N$ , it either vanishes (stable) or diverges (unstable). These asymptotic effects are pronounced more strongly as  $S$  becomes more negative or more positive. As an example, let us compare Regulatory with  $h = 1, a = 2$ , under which we have  $S = -\beta/2$ , vs. Population 1, where  $S = -\beta$ . Both are asymptotically stable, yet Eq. (10) indicates that Population 1 is *more* stable: to destabilize Population 1 one needs  $C_0^{\text{Pop}} \sim N^{-\beta}$ , while for Regulatory it is sufficient to have  $C_0^{\text{Reg}} \sim N^{-\beta/2}$ , *i.e.*  $C_0^{\text{Pop}} \ll C_0^{\text{Reg}}$ . The meaning is that to destabilize Population 1 we much push  $C$  further towards zero, namely set more extreme parameters, than what is needed for Regulatory.

In Fig. 6b we show the lines of *equi-stability*, comprising all dynamics with the same  $S$  value, and hence a similar level of stability/instability. These equi-stable classes may group together highly distinct dynamics, that despite their different  $\Omega$  may have identical  $S$ . For example, Epidemic and Population 1, two dynamics from fundamentally different domains, exhibit a similar level of stability, belonging to the *equivalence stability class*  $S = -\beta$ .

**Generality and limitations the  $\mathbb{E}(A, G, \Omega)$  ensemble.** Our ensemble  $\mathbb{E}(A, G, \Omega)$  was obtained and analyzed under the conditions defined by Eq. (3), whose structure allowed us to achieve the reported analytical advances. Despite its general structure, this equation excludes several

families of dynamics. For example, non-additive interactions or threshold models.<sup>50</sup> Similarly, if the system incorporates a mixture of distinct interaction mechanisms its dynamics cannot be cast into the form  $\mathbf{M}$ .

We note, however, that while our analytical derivations are, indeed, bounded by these restrictions, the family of potential dynamics included in  $\mathbb{E}(A, G, \Omega)$  may, in fact, be broader. Specifically, in Supplementary Section 4 we consider three expansions to Eq. (3) • *Non-factorizable interactions*. Our testing ground includes Power dynamics, in which the interaction term cannot be partitioned into a product  $M_1(x_i)M_2(x_j)$ , but rather incorporates a diffusive mechanism of the form  $M(x_j - x_i)$ . Such dynamics, excluded from (3), arise in different contexts, from reaction-diffusion to synchronization,<sup>51,52</sup> and despite the fact that they are not covered by our analytical framework, our analysis of Power indicates that they continue to fall within  $\mathbb{E}(A, G, \Omega)$  • *Non-additive interactions*. Another outlier in Fig. 2 is Population 2, in which the linear sum over  $M_2(x_j)$  is replaced by  $M_2(\sum_{j=1}^N x_j)$ . This represents a common structure in population dynamics, which, as our analysis shows, is also within the  $\mathbb{E}(A, G, \Omega)$  family • *Mixed s dynamics*. While Eq. (3) is limited to uniform dynamics, either cooperative ( $\mathbf{s} = 1$ ) or adversarial ( $\mathbf{s} = 0$ ), in Supplementary Section 4.3 we numerically analyze the case of mixed dynamics, in which a fraction  $\phi$  of cooperative interactions coexists alongside a  $1 - \phi$  fraction of adversarial ones. We find that for a broad range of  $\phi$  values, our predicted Jacobian patterns remain valid. This is thanks to a constraint relevant in many real-world systems: the fact that the activities  $x_i(t)$  in (3) are, by definition, non-negative.<sup>21,22</sup> Therefore, as the system evolves in time, at any instance where a node reaches  $x_i(t) = 0$  it becomes extinct, and permanently removed from the network. This *ratchet-motion* prunes out nodes with many adversarial interacting partners, as their activities are naturally driven towards zero. As a result, the system reaches a fixed-point in which the majority of remaining links are positive, which continue to approximately follow Eqs. (4) and (5) of the  $\mathbb{E}(A, G, \Omega)$  ensemble.

## Discussion and outlook

The linear stability matrix  $J$  carries crucial information on the dynamic behavior of complex systems. Here, we exposed distinct patterns in the structure of  $J$  that (i) arise from the nature of the system’s interaction dynamics; (ii) affect its principal eigenvalue, and thus, its stability profile. These patterns are expressed through the four dynamic exponents  $\Omega = (\eta, \mu, \nu, \rho)$ , which we link to the system’s dynamics,  $\mathbf{M}$ , through the leading powers of the expansions in Eq. (12). This dependence on the *powers* ( $\Psi(n), \Gamma(n)$ , etc.), rather than the *coefficients* ( $G_n, C_n$ , etc.) indicates that  $\Omega$  is hardwired into the interaction dynamics. Indeed, the powers in (12) are determined by the dynamic model, *e.g.*, Epidemic or Regulatory, but not by the specific model parameters, which only impact the coefficients. Therefore, our predicted Jacobian ensemble in (4) and (5), as well as its associated stability classifier  $S$  in (9), both capture highly robust and distinctive characteristics of the system’s dynamics, that cannot be perturbed or otherwise affected by shifting environmental conditions.

External forces, however, may not only impact the system’s structure ( $A, G$ ) or parameters ( $\mathbf{f}, \mathcal{G}$ ), but also directly act on the node dynamics. This, for example, arises in non-autonomous systems, in which the nodes interact with components outside the network. Such effects can be captured in Eq. (3) by coupling it with a *virtual* node/s, whose activities  $z_i(t)$  are designed to encapsulate the dynamic impact of the external signals. As long as the number of these external coupling terms is small, *i.e.* weak environmental forces, our  $J$  will only be marginally affected.

Graph spectral analysis represents a central mathematical tool to translate network structure

into dynamic predictions.<sup>53–55</sup> A network’s spectrum, *i.e.* its set of eigenvalues and eigenvectors, captures information on its dynamic time-scales, potential states, and - in the present context - its dynamic stability. Most often, spectral analysis is applied to the network *topology*, namely we seek the *graph’s* eigenvalues. Focusing on the graph topology, however, loses information on the nonlinear dynamics that occur *on* that graph. As an alternative, our  $\mathbb{E}(A, G, \Omega)$  ensemble suggests to apply spectral analysis, not to the topology  $A$  (or the weighted  $A \otimes G$ ), but rather to the derived Jacobian in (4) and (5), which, thanks to  $\Omega$  preserves the information of both structure *and* dynamics.

In a broader perspective, the interplay between topology and dynamics is one of the major theoretical obstacles along the path to predict, understand and control complex system behavior.<sup>56–59</sup> The problem is that we lack sufficient theoretical tools to treat the challenging combination of nonlinear dynamics with complex, random and often highly heterogeneous network structures. Consequently, advances are often system specific, requiring dedicated tools, and hence, lacking the breadth of a general network dynamics theory. The Jacobian ensemble presented here, transforms the nonlinear Eq. (3) into an effective linear system, whose weights incorporate the nonlinear  $\mathbf{M}$  through  $\Omega$ . It can, therefore, allow us to utilize the powerful tools of spectral graph theory, even in a nonlinear dynamic setting. This may offer a basis for systematic analysis of nonlinear network dynamics.

**Code and data availability.** Upon acceptance, all codes/data to reproduce our analysis will be made freely available online.

**Acknowledgments.** C.M. thanks the Planning and Budgeting Committee (PBC) of the Council for Higher Education, Israel for support. C.M. is also supported by the INSPIRE-Faculty grant (code: IFA19-PH248) of the Dept. of Science and Technology, India. C.H. is supported by the INSPIRE-Faculty grant (code: IFA17-PH193) of the Dept. of Science and Technology, India. S.B. acknowledges funding from the project EXPLICS granted by the Italian Ministry of Foreign Affairs and International Cooperation. This research was also supported by the Israel Science Foundation (grant No. 499/19), the US National Science Foundation-CRISP award No. 1735505, and by the Bar-Ilan University Data Science Institute grant for data science research.

## Appendix I. The ensemble $\mathbb{E}(A, G, \Omega)$ - how to calculate $\Omega$

To construct  $J$  as appears in Eqs. (4) and (5) we must extract the exponents  $\Omega = (\eta, \mu, \nu, \rho)$  from Eq. (3). First we use the dynamic functions  $M_0(x), M_1(x)$  and  $M_2(x)$  to construct three new functions

$$R(x) = -\frac{M_1(x)}{M_0(x)}, \quad Y(x) = M_1(x)R'(x), \quad Z(x) = R(x)M_2(x), \quad (11)$$

where  $R'(x)$  represents a derivative  $dR/dx$  around the fixed-point  $\mathbf{x}$ . From these we extract four additional functions, which we express through a Hahn power-series expansion as

$$\begin{aligned} M_2(Z^{-1}(x)) &= \sum_{n=0}^{\infty} G_n x^{\Psi(n)}, & Y(R^{-1}(x)) &= \sum_{n=0}^{\infty} C_n x^{\Gamma(n)}, \\ M_1(R^{-1}(x)) &= \sum_{n=0}^{\infty} K_n x^{\Pi(n)}, & M'_2(R^{-1}(x)) &= \sum_{n=0}^{\infty} L_n x^{\Theta(n)} \end{aligned}, \quad (12)$$

where  $R^{-1}(x)$  and  $Z^{-1}(x)$  represent the inverse functions of  $R(x)$  and  $Z(x)$ . The Hahn expansion<sup>60</sup> is a generalization of the Taylor expansion to include negative and real powers. Hence  $\Psi(n), \Gamma(n), \Pi(n)$  and  $\Theta(n)$  represent series of real powers in ascending order, the leading (*i.e.* smallest) powers assigned the index  $n = 0$ . These leading powers directly provide  $\Omega$  via

$$\mu = 2 - \Gamma(0), \quad \nu = -\Pi(0), \quad \rho = -\Theta(0), \quad \eta = -\Psi(0)(\mu - \nu - \rho). \quad (13)$$

Hence, to construct  $J \in \mathbb{E}(A, G, \Omega)$  we first generate the weighted network  $A \otimes G$ , then extract the weighted degrees  $d_i$  of all nodes and the nearest neighbor degree  $\mathcal{D}_{nn}$  of Eq. (6). The resulting  $J$  satisfies

$$J_{ii} \sim -C(\mathbf{f}, \mathcal{G}) \mathcal{D}_{nn}^{\eta} d_i^{\mu} \quad (14)$$

$$J_{ij} \sim d_i^{\nu} A_{ij} G_{ij} d_j^{\rho}, \quad (15)$$

where the constant  $C > 0$  captures the system's specific dynamic time-scales. Note that  $\Omega$ , as opposed to  $C$ , depends only on the leading *powers* of (12), and not on the *coefficients*. Therefore it is unaffected by Eq. (3)'s microscopic parameters, but rather captures an intrinsic characteristic of each dynamic *model*. Namely  $\Omega$  distinguished between, *e.g.*, Epidemic and Regulatory, but remains the same under two Epidemic systems with different recovery/infection rates. The detailed derivation of  $\Omega$  appears in Supplementary Section 1, followed by a step by step application on all our testing ground dynamics (Fig. 2) in Supplementary Section 3.

In the above formulation we have assumed that  $R(x)$  and  $Z(x)$  are invertible, writing  $R^{-1}(x)$  and  $Z^{-1}(x)$  in (12). In Supplementary Section 1 we explain how to properly treat non-invertible  $R(x), Z(x)$ . In these sections, we also demonstrate how to extract  $J$  for system's with multiple fixed-points, and, specifically, in Supplementary Section 1.5, how to construct  $J$  around a trivial fixed-point  $\mathbf{x} = (0, \dots, 0)^{\top}$ .

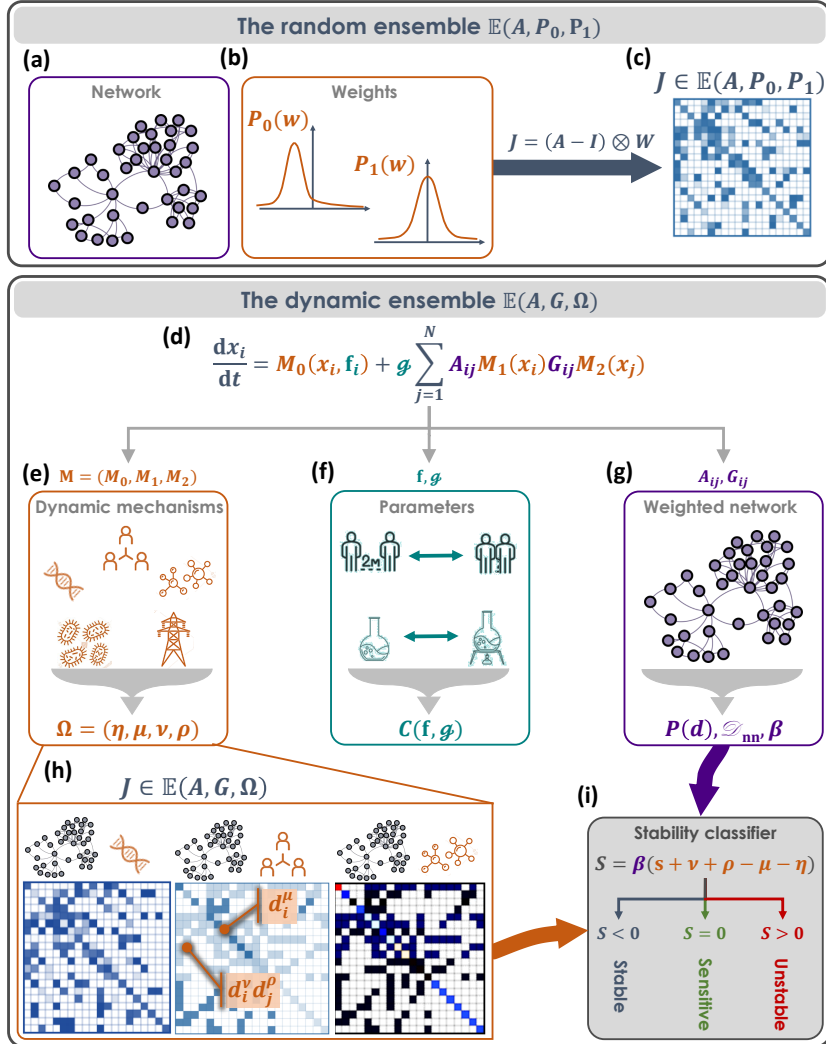


**Figure 1: The dynamic Jacobian ensemble.** To predict dynamic stability we seek the system's stability matrix  $J$ . (a)-(b) The classic approach is to structure  $J$  around the network topology  $A$ , with weights extracted from two distributions:  $P_0(w)$  for the diagonal entries  $J_{ii}$  (typically negative) and  $P_1(w)$  for the interactions strengths  $J_{ij}$ ,  $i \neq j$ .  $P_0(w), P_1(w)$  are designed to capture the typical time-scales of the system's self/interaction dynamics. (c) Together this provides  $J \in \mathbb{E}(A, P_0, P_1)$ , a random matrix based construction, whose stability is determined by the the structure  $A$  and the random weights  $W$ . (d) Such construction, however, disregards the system's intrinsic interaction *mechanisms*, *e.g.*, infection/recovery (Epidemic) or activation/inhibition (Regulatory). We therefore derive  $J$  directly from the nonlinear Eq. (3), which models network dynamics using a composition of three distinct factors: (e) The dynamic mechanisms (orange) are captured by the nonlinear form of the functions  $\mathbf{M}$ . These mechanisms are *hardwired* into the system's interacting components, hence unaffected by external perturbations. Our formalism derives the exponents  $\Omega$  in Eqs. (4) and (5) directly from  $\mathbf{M}$ . (f) The system's microscopic parameters  $\mathbf{f}, \mathcal{G}$  (turquoise) provide the specific rate-constants for (3)'s dynamic processes. For example, the infection rate in Epidemic (top), or the degradation rate in Biochemical (bottom). These parameters are non-intrinsic, and therefore, influenced by external conditions, such as changes in social behavior (Epidemic) or temperature (Biochemical). Their impact on  $J$  is encapsulated within the coefficient  $C(\mathbf{f}, \mathcal{G})$  in Eq. (4). (g)  $A, G$  represent the weighted network (purple), which is expressed in  $J$  via the weighted degree distribution  $P(d)$ , the nearest neighbor degree  $\mathcal{D}_{nn}$  in (6) and  $\beta$  in (7). (h) The resulting  $J$ -ensemble,  $\mathbb{E}(A, G, \Omega)$ , exhibits non-random scaling patterns driven by the the interplay between  $A, G$  and  $\Omega$ . Similar to the random  $\mathbb{E}(A, P_0, P_1)$ , the non-vanishing terms correspond to the network links, however, in contrast to the random weight assignment of  $\mathbb{E}(A, P_0, P_1)$ , here the weight of the  $i, j$  entry depends on  $d_i$  and  $d_j$ , as well as on  $\Omega$  (orange captions). The result is a *dynamic* ensemble, in which identical networks ( $A, G$ ) yield highly distinctive  $J$  matrices depending on  $\mathbf{M}$ , *e.g.*, Regulatory (left), Epidemic (center) or Biochemical (right). (i) The stability of  $J$  can be reduced to the classifier  $S$  in (9), whose value depends only on the degree heterogeneity ( $\beta$ , purple) and on the dynamic exponents (orange terms), but not the parameters  $\mathbf{f}, \mathcal{G}$ . Therefore, it provides a robust classification into stable (blue) or unstable (red) dynamics, that are asymptotically insensitive to changes in environmental conditions, *i.e.* parameters  $\mathbf{f}, \mathcal{G}$ . Under  $S = 0$  the system becomes sensitive (green), in which case stability is driven by the potentially tunable parameters.

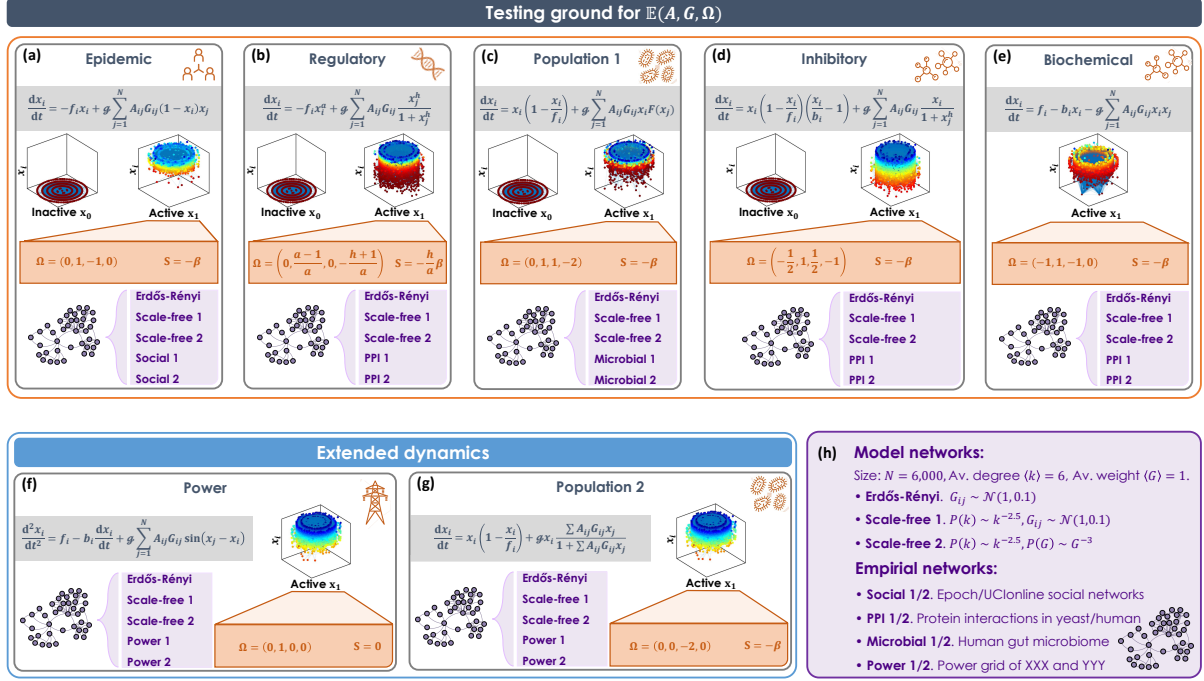


**Figure 2: Testing ground for the  $\mathbb{E}(A, G, \Omega)$  ensemble.** We constructed different combinations of (weighted) networks  $A, G$  and dynamics  $\mathbf{M}$  to examine our  $J$ -ensemble. (a) Epidemic. We implemented the susceptible-infected-susceptible (SIS) dynamics (grey box) on a set of model and real-world networks (violet box). This system exhibits two potential fixed-points (3D plots): the inactive  $\mathbf{x}_0$ , in which all activities vanish, *i.e.* healthy, and the active  $\mathbf{x}_1$ , in which all  $x_i > 0$ , namely the pandemic state. In this 3D visualization the nodes  $i = 1, \dots, N$  are laid out on the  $x, y$  plane and their fixed-point activity  $x_i$  is represented by color (red - low, blue - high) and vertical displacement ( $z$ -axis). Therefore, in  $\mathbf{x}_0$  all nodes are on the  $x, y$  plane ( $x_i = 0$ ), and in  $\mathbf{x}_1$  they are distributed along  $z > 0$  and range from red to blue. In each of these states the system has a different set of exponents  $\Omega$  and hence a different Jacobian  $J$ . Here we present  $\Omega$  and  $S$  for the non-vanishing state  $\mathbf{x}_1$  (orange box). The remaining panels follow a similar format. (b) Regulatory. Sub-cellular dynamics following the Michaelis-Menten model. (c) Population 1. Mutualistic interactions in, *e.g.*, microbial communities. (d) Inhibitory. Suppression dynamics, *e.g.*, between hosts and pathogens. (e) Biochemical. Protein-protein interactions modeled via mass-action kinetics. This system exhibits a single fixed-point, and therefore includes a single 3D plot. (f) Power. Synchronization dynamics between power system components. (g) Population 2. Mutualistic population dynamics with non-additive interactions, namely replacing the term  $\sum_{j=1}^N A_{ij} G_{ij} M_2(x_j)$  in Eq. (3) by  $M_2(\sum_{j=1}^N A_{ij} G_{ij} x_j)$ . (h) Our model and empirical networks. For a detailed description of all networks see Supplementary Section 5.4. Together we arrive at a set of 35 combinations of networks/dynamics upon which we test our theoretical framework. A detailed analysis of all dynamic models appears in Supplementary Section 3. Note that Population 2 and Power are not in the form of Eq. (3), and hence they expand our testing ground beyond the bounds of our analytical framework. We provide a dedicated analysis of these models, together with a mixed-dynamics scenario in Supplementary Section 4.

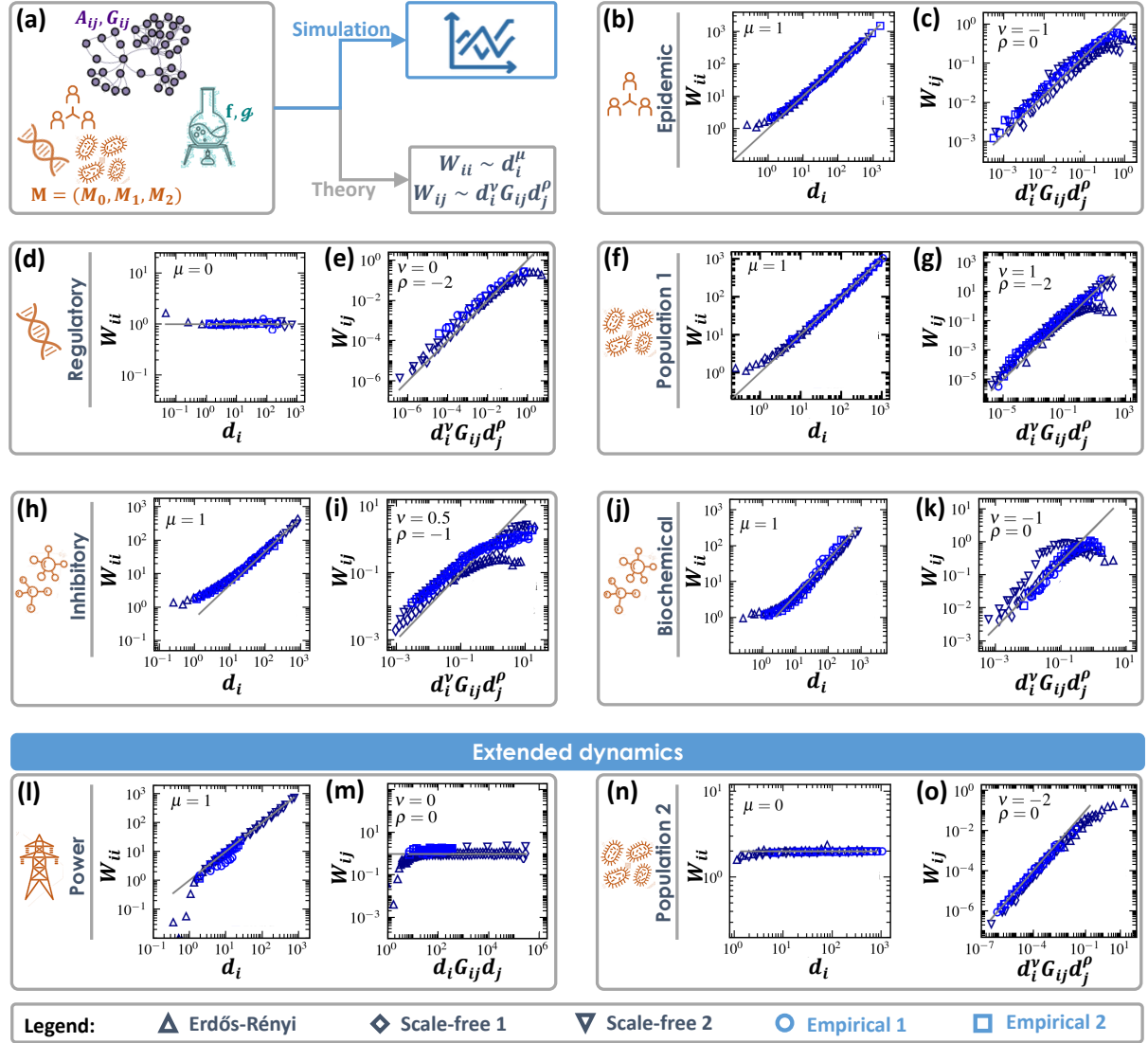


Figure 3: **Emergent patterns in the dynamic ensemble  $\mathbb{E}(A, G, \Omega)$ .** We implemented our seven dynamic models, Epidemic, Regulatory, Population 1 etc., on a set of relevant model and empirical networks, as detailed in our testing ground of Fig. 2. Focusing on the non-vanishing state  $\mathbf{x}_1$ , we perturbed all nodes around their numerically obtained fixed-point to construct the Jacobian,  $J$ . (a) The numerical simulations incorporate the full complexity of Eq. (3), including the weighted network (purple), the diverse parameters (green) and the nonlinear mechanisms (orange). This helps us observe the *real* Jacobian matrices for each of our systems, as obtained from actual numerical runs of the nonlinear network models (Simulation, blue, top). We then compare in each panel the simulation results with our theoretical predictions based on the  $\mathbb{E}(A, G, \Omega)$  ensemble (Theory, grey, bottom). (b) The diagonal weights  $W_{ii}$  vs. the weighted degree  $d_i$  as obtained from Epidemic dynamics (symbols). We observe the scaling relationship of Eq. (4) with  $\mu = 1$  (grey solid line) confirming our predicted  $J$ -patterns for this dynamics. We also find that this scaling is independent of the specific network, intrinsic to the Epidemic dynamics, as predicted. (c) The off-diagonal weights  $W_{ij}$  vs. prediction (5) with  $\nu = -1, \rho = 0$  (symbols). Once again, we observe a perfect agreement with our theoretical prediction (grey solid line). We also include results obtained from two relevant empirical networks, Social 1 and Social 2 (light blue circles/squares), capturing online social dynamics. (d)-(e) Similar results are observed under Regulatory dynamics ( $\mu = \nu = 0, \rho = -2$ ) on both model and real networks (PPI 1 and PPI 2); (f)-(g) Population 1 dynamics ( $\mu = \nu = 1, \rho = -2$ , empirical networks: Microbial 1 and Microbial 2); (h)-(i) Inhibitory dynamics ( $\mu = 1, \nu = 1/2, \rho = -1$ , empirical networks: PPI 1 and PPI 2); (j)-(k) Biochemical dynamics ( $\mu = 1, \nu = -1, \rho = 0$ , empirical networks: PPI 1 and PPI 2). (l)-(m) Power dynamics ( $\mu = 1, \nu = \rho = 0$ , empirical networks: Power 1 and Power 2); (n)-(o) Population 2 dynamics ( $\mu = 0, \nu = -2, \rho = 0$ , empirical networks: Microbial 1 and Microbial 2); As predicted, we find that real Jacobian matrices exhibit the non-random patterns of Eqs. (4) and (5), and therefore cannot be modeled via the random ensemble  $\mathbb{E}(A, P_0, P_1)$ , but rather through our dynamic Jacobian family  $\mathbb{E}(A, G, \Omega)$ . Data in all panels are logarithmically binned.<sup>61</sup> Details on the numerical calculation of  $J$ , log-binning and the construction of all model/real networks appear in Supplementary Section 5.

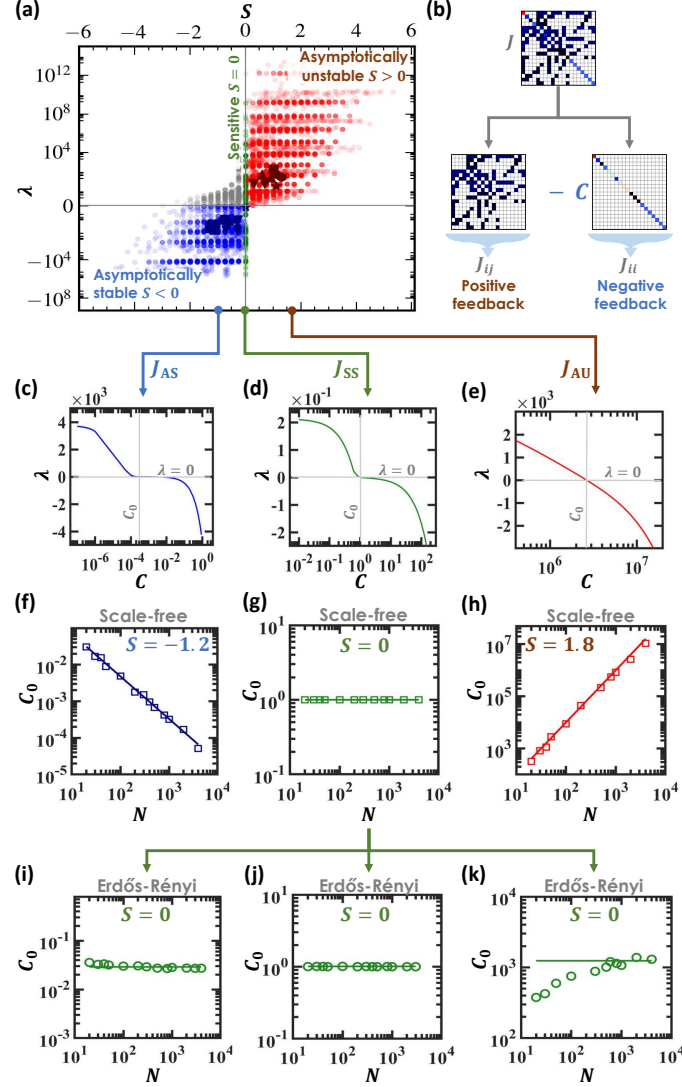


Figure 4: **Three classes of dynamic stability in real and model networks.** We extracted 7,387 Jacobian matrices from the  $\mathbb{E}(A, G, \Omega)$  ensemble, using combinations of model/real networks with different dynamic exponents  $\Omega$ . For each  $J$  we calculated the principal eigenvalue  $\lambda$  and the stability classifier  $S$  in (9). (a)  $\lambda$  vs.  $S$  for all 7,387  $J$ -matrices. We observe the three predicted classes: Asymptotically unstable (red) in which  $S > 0$  and hence also  $\lambda > 0$ ; Sensitively stable (green), where  $S = 0$  and  $\lambda$  can be both positive or negative; Asymptotically stable (blue), where  $S < 0$  and therefore  $\lambda < 0$ . Our classification was inaccurate in  $\sim 4\%$  of the cases on binary networks,  $\sim 5\%$  on weighted networks and  $\sim 15\%$  on weighted/negative networks, amounting to a total discrepancy of  $\sim 8\%$  over the entire ensemble (grey dots). Empirical networks (solid symbols): Under the random ensemble  $\mathbb{E}(A, P_0, P_1)$  all our empirical networks are classified as unstable (red symbols). This is a consequence of the diversity-stability principle that predicts, for random networks, an asymptotic instability (see **Box I**). However, the same networks under  $\mathbb{E}(A, G, \Omega)$ , each with its relevant  $\Omega$ , become dynamically stable (blue symbols). Hence, networks rendered unstable via the existing random matrix paradigm, are, in fact, stable, when accounting for the nonlinearity through  $\Omega$ . (b) The value of  $\lambda$  emerges from the competition between  $J$ 's off-diagonal terms, representing positive feedback, and the strength of the diagonal terms  $J_{ii}$  (negative feedback). Therefore one can force a system towards stability ( $\lambda < 0$ ) by increasing  $C$  in (4). (c)-(e) Taking three specific  $J$  matrices from each class, we plot  $\lambda$  vs.  $C$ , seeking the critical  $C_0$ , in which  $\lambda$  becomes negative (grey lines). (f) For the stable  $J_{AS}$  ( $S = -1.2$ ) we find that  $C_0$  decreases with  $N$  (squares), capturing the asymptotic stability, in which for large systems ( $N \rightarrow \infty$ ) stability is sustained even under arbitrarily small  $C$ . The theoretical scaling predicted in Eq. (10) is also shown (solid line, slope  $-1.2$ ). (g) For  $J_{SS}$  we have  $S = 0$ , the critical  $C_0$  is independent of  $N$ , hence the system's stability can be affected by finite changes to its dynamic parameters, *e.g.*, environmental perturbations. (h) The asymptotically unstable  $J_{AU}$  ( $S = 1.8$ ) has  $C_0 \rightarrow \infty$  in the limit of large  $N$ , in perfect agreement with Eq. (10) (solid line). (i)-(k) For a bounded  $P(d)$ , *e.g.*, Erdős-Rényi,  $\beta$  vanishes and hence  $S = 0$  in (9). Under these conditions, regardless of  $\Omega$ , the system is always sensitively stable and therefore  $C_0$  does not scale with  $N$ . This demonstrates the role of degree-heterogeneity in ensuring stability, in the face of changing environmental conditions.

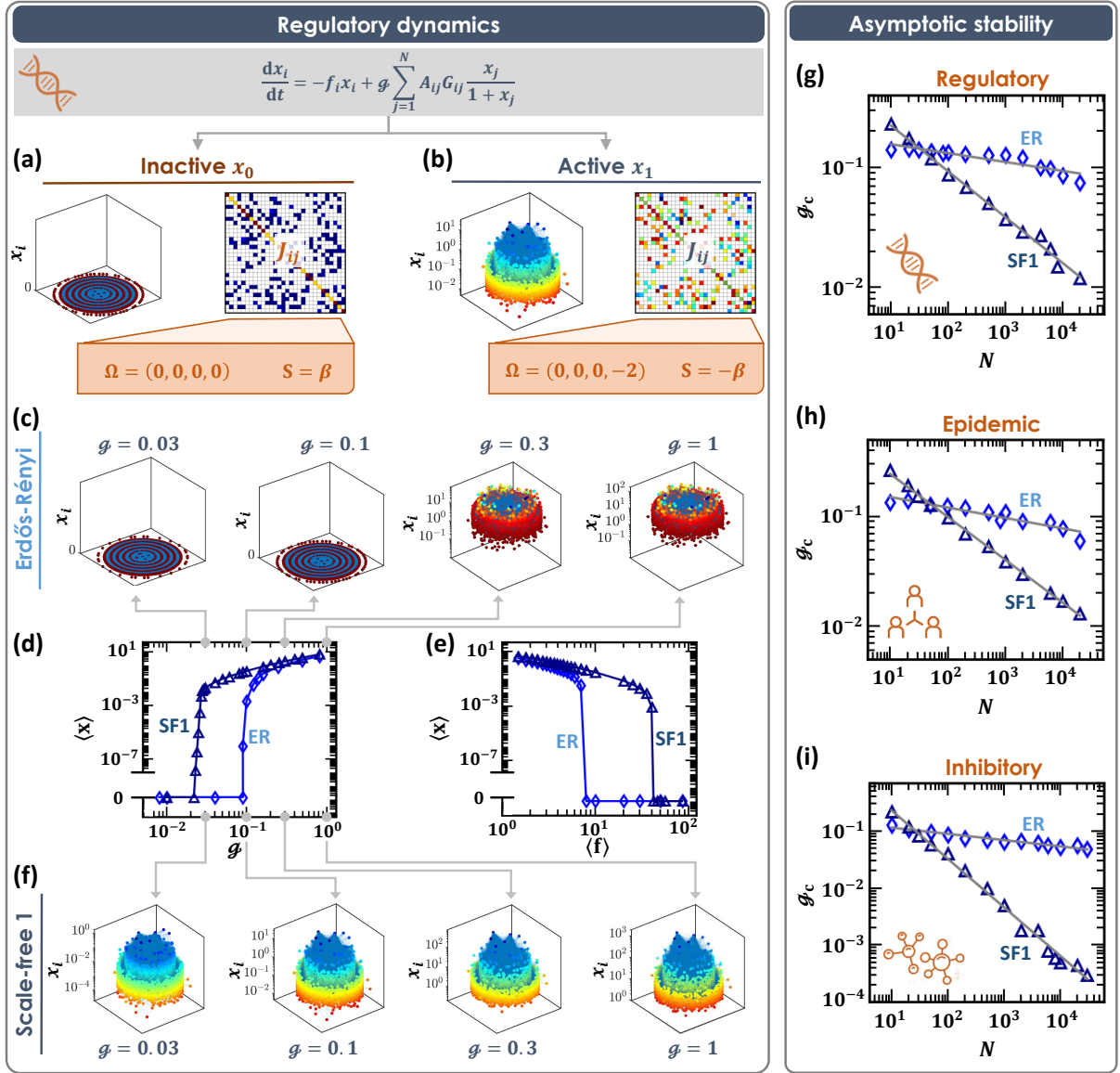


Figure 5: **Emergent stability in large heterogeneous networks.** (a)-(b) Regulatory dynamics exhibit two fixed points (3D plots), each with its own  $J \in \mathbb{E}(A, G, \Omega)$ , shown to the right of each plot. The inactive  $\mathbf{x}_0$  has  $\Omega = (0, 0, 0, 0)$  and  $S = \beta > 0$ , and hence it is asymptotically unstable. The active  $\mathbf{x}_1$  has a different  $J$ , with  $\Omega = (0, 0, 0, -2)$  and  $S = -\beta < 0$ , asymptotically stable. (c) The state of Regulatory as obtained from numerical simulations on our ER network under varying  $\mathcal{G}$ . The system transitions from  $\mathbf{x}_1$  (right) to  $\mathbf{x}_0$  (left) under small  $\mathcal{G}$ . This represents sensitive stability, as indeed predicted for ER, in which parameters, here  $\mathcal{G}$ , affect the state of the system. (d) To examine this systematically we plot the mean activity  $\langle \mathbf{x} \rangle$  vs.  $\mathcal{G}$  as obtained for ER (diamonds) and for our scale-free network SF1 (triangles). Both systems exhibit a critical  $\mathcal{G}_c$ , below which  $\mathbf{x}_1$  becomes unstable and the system transitions to  $\mathbf{x}_0$ . The crucial point is, however, that thanks to its heterogeneity SF1 exhibits an increased robustness against  $\mathcal{G}$  variations, with  $\mathcal{G}_c$  an order of magnitude lower than that observed for ER. (e)  $\langle \mathbf{x} \rangle$  vs.  $\langle \mathbf{f} \rangle$  shows a similar behavior. Here *increasing*  $\langle \mathbf{f} \rangle$  causes the system to collapse to  $\mathbf{x}_0$ , and, as predicted, SF1 can incur higher  $\langle \mathbf{f} \rangle$  than ER. (f) The state of SF1 under the same four conditions ( $\langle \mathbf{f} \rangle, \mathcal{G}$ ) as shown in panel (c) for ER. Indeed, SF1 remains at  $\mathbf{x}_1$  even when ER has already collapsed to  $\mathbf{x}_0$ . (g)  $\mathcal{G}_c$  vs. the system size  $N$  as obtained from numerically simulating Regulatory dynamics. For ER we observe  $\mathcal{G}_c \sim \text{const}$  (diamonds), *i.e.* the system *can* be destabilized via parameter perturbation. Indeed, while  $N$  spans over four orders of magnitude,  $\mathcal{G}_c$  varies by a mere  $\sim 40\%$ . In contrast, for SF1 we find that  $\mathcal{G}_c$  exhibits negative scaling with  $N$ , approaching  $\mathcal{G}_c \rightarrow 0$  in the limit  $N \rightarrow \infty$ . This captures precisely the predicted asymptotic stability, in which a sufficiently large and heterogeneous network is guaranteed to stably reside in  $\mathbf{x}_1$ . (h)-(i) Repeating this experiment for Epidemic and Inhibitory, we continue to observe our predicted asymptotic stability. For  $N \rightarrow \infty$  we have  $\mathcal{G}_c \rightarrow 0$  under the heterogeneous SF1, vs.  $\mathcal{G}_c$  independent of  $N$  under the homogeneous ER.

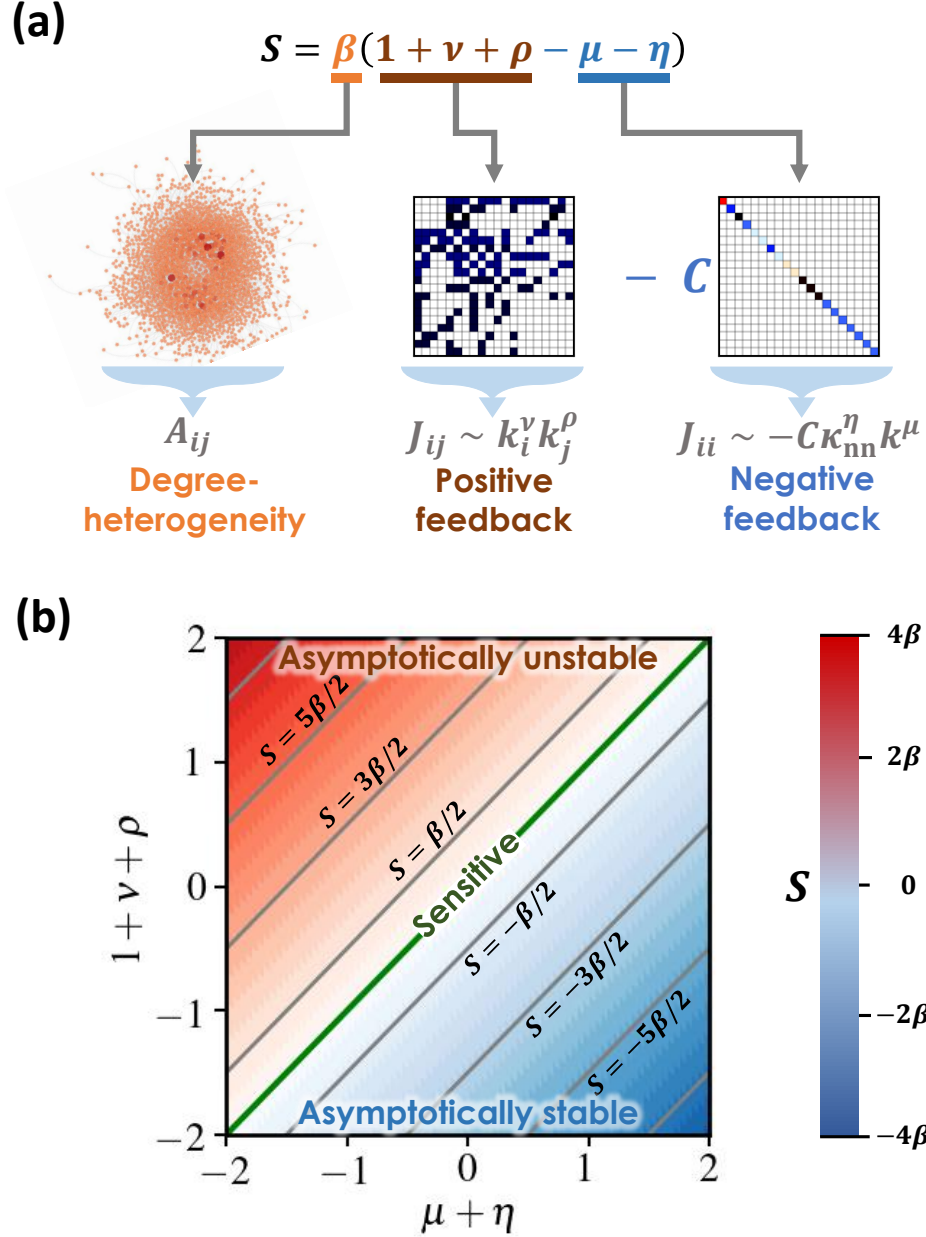


Figure 6: **The ingredients of dynamic stability.** (a) The stability classifier  $S$  (9) comprises five exponents:  $\beta$  characterizes the network topology and its degree heterogeneity via (7);  $\nu, \rho$  determine the magnitude of  $J$ 's off-diagonal terms  $J_{ij}$ ;  $\mu, \eta$  characterize the diagonal terms  $J_{ii}$ , *i.e.* each node's self-regulation. This portrays stability as a balance between the positive feedback mediated by the system's interactions, strengthened with increasing  $\nu, \rho$ , vs. the stabilizing effect of the diagonal terms, that are reinforced by  $\eta, \mu$ . Indeed,  $S$  in (9) tends to be positive, *i.e.* unstable, with increasing  $\nu, \rho$ , and negative, *i.e.* stable, with increasing  $\eta, \mu$ . (b)  $S$  (color-bar) vs. the exponents  $\Omega = (\eta, \mu, \nu, \rho)$ . Indeed, increasing  $\nu, \rho$  drives the system towards the unstable class ( $S > 0$ , red), while increasing  $\mu, \eta$  enhances the system's stability (blue). In addition to the discrete classification of stable dynamics (blue,  $S < 0$ ), unstable dynamics (red,  $S > 0$ ) and sensitive dynamics (green,  $S = 0$ ),  $S$  also helps quantify the continuum *level* of stability, where the more negative/positive is  $S$ , the more stable/unstable is the system. Grey lines represent *equi-stable* systems. We find that highly distinct dynamical systems may reside within the same *equi-stability* class.

## References

- [1] S.V. Buldyrev, R. Parshani, G. Paul, H.E. Stanley and S. Havlin. Catastrophic cascade of failures in interdependent networks. *Nature*, 464:1025–1028, 2010.
- [2] I. Dobson, B.A. Carreras, V.E. Lynch and D.E. Newman. Complex systems analysis of series of blackouts: Cascading failure, critical points, and self-organization. *Chaos*, 17:026103, 2007.
- [3] D. Duan, C. Lv, S. Si, Z. Wang, D. Li, J. Gao, S. Havlin, H.E. Stanley and S. Boccaletti. Universal behavior of cascading failures in interdependent networks. *Proc. Natl. Acad. Sci. USA*, 116:22452–57, 2019.
- [4] A.E. Motter and Y.-C. Lai. Cascade-based attacks on complex networks. *Physical Review E*, 66:065102, 2002.
- [5] P. Crucitti, V. Latora and M. Marchiori. Model for cascading failures in complex networks. *Phys. Rev. E*, 69:045104–7, 2004.
- [6] D. Achlioptas, R.M. D’Souza and J. Spencer. Explosive percolation in random networks. *Science*, 323:1453–1455, 2009.
- [7] J. Gao, B. Barzel and A.-L. Barabási. Universal resilience patterns in complex networks. *Nature*, 530:307–312, 2016.
- [8] S. Boccaletti, J.A. Almendral, S. Guama, I. Leyvad, Z. Liua, I.S. Nadal, Z. Wang and Y. Zou. Explosive transitions in complex networks’ structure and dynamics: Percolation and synchronization. *Physics Reports*, 660:1–94, 2016.
- [9] S. Boccaletti, V. Latora, Y. Moreno, M. Chavez and D.-U. Hwang. Complex networks: Structure and dynamics. *Physics Reports*, 424:175–308, 2006.
- [10] Michael M Danziger, Ivan Bonamassa, Stefano Boccaletti, and Shlomo Havlin. Dynamic interdependence and competition in multilayer networks. *Nature Physics*, 15(2):178–185, 2019.
- [11] K.Z. Coyte, J. Schluter and K.R. Foster. The ecology of the microbiome: Networks, competition, and stability. *Science*, 350:663–666, 2015.
- [12] R.V. Solé and J.M. Montoya. Complexity and fragility in ecological networks. *Proc. R. Soc. London Ser. B*, 268:2039–2045, 2001.
- [13] H.I. Schreier, Y. Soen and N. Brenner. Exploratory adaptation in large random networks. *Nature Communications*, 8:14826, 2017.
- [14] L.M. Pecora and T.L. Carroll. Master stability functions for synchronized coupled systems. *Phys. Rev. Lett.*, 80:2109, 1998.
- [15] V.I. Arnold. *Ordinary Differential Equations*. MIT Press, Cambridge, MA, 1973.
- [16] M.W. Hirsch and S. Smale. *Differential Equations, Dynamical Systems and Linear Algebra*. Academic Press, New York, 1974.
- [17] B. Barzel and O. Biham. Quantifying the connectivity of a network: The network correlation function method. *Phys. Rev. E*, 80:046104–15, 2009.
- [18] R.M. May. Will a large complex system be stable? *Nature*, 238:413 – 414, 1972.
- [19] G. Yan, N.D. Martinez and Y.-Y. Liu. Degree heterogeneity and stability of ecological networks. *Journal of The Royal Society Interface*, 14:131, 2017.
- [20] K.S. McCann. The diversity–stability debate. *Nature*, 405(6783):228–233, 2000.
- [21] J.D. O’Sullivan, R.J. Knell and A.G. Rossberg. Metacommunity-scale biodiversity regulation and the self-organised emergence of macroecological patterns. *Ecology Letters*, 22:1428, 2019.
- [22] M. Barbier, C. de Mazancourt, M. Loreau and G. Bunin. *Phys. Rev. X*, 11:011009, 2021.
- [23] G. Caldarelli. *Scale-free networks: complex webs in nature and technology*. Oxford University Press, New York, 2007.
- [24] B. Barzel and A.-L. Barabási. Universality in network dynamics. *Nature Physics*, 9:673 – 681, 2013.
- [25] U. Harush and B. Barzel. Dynamic patterns of information flow in complex networks. *Nature Communications*, 8:2181, 2017.
- [26] C. Hens, U. Harush, R. Cohen, S. Haber and B. Barzel. Spatiotemporal propagation of signals in complex networks. *Nature Physics*, 15:403, 2019.

[27] R. Pastor-Satorras, C. Castellano, P. Van Mieghem and A. Vespignani. Epidemic processes in complex networks. *Rev. Mod. Phys.*, 87:925–958, 2015.

[28] P.S. Dodds, R. Muhamad and D.J. Watts. An experimental study of search in global social networks. *Science*, 301:827–829, 2003.

[29] D. Brockmann, V. David and A.M. Gallardo. Human mobility and spatial disease dynamics. *Reviews of Nonlinear Dynamics and Complexity*, 2:1, 2009.

[30] G. Karlebach and R. Shamir. Modelling and analysis of gene regulatory networks. *Nature Reviews*, 9:770–780, 2008.

[31] J.D. Murray. *Mathematical Biology*. Springer, Berlin, 1989.

[32] B. Barzel and O. Biham. Binomial moment equations for stochastic reaction systems. *Phys. Rev. Lett.*, 106:150602–5, 2011.

[33] B. Barzel and O. Biham. Stochastic analysis of complex reaction networks using binomial moment equations. *Phys. Rev. E*, 86:031126, 2012.

[34] C.S. Holling. Some characteristics of simple types of predation and parasitism. *The Canadian Entomologist*, 91:385–398, 1959.

[35] J.N. Holland, D.L. DeAngelis and J.L. Bronstein. Population dynamics and mutualism: functional responses of benefits and costs. *American Naturalist*, 159:231–244, 2002.

[36] D. Wodarz, J.P. Christensen and A.R. Thomsen. The importance of lytic and nonlytic immune responses in viral infections. *Trends in Immunology*, 23:194–200, 2002.

[37] E.L. Berlow, J.A. Dunne, N.D. Martinez, P.B. Stark, R.J. Williams and U. Brose. Simple prediction of interaction strengths in complex food webs. *Proceedings of the National Academy of Sciences*, 106:187–191, 2009.

[38] J.F. Hayes and T.V.J. Ganesh Babu. *Modeling and Analysis of Telecommunications Networks*. John Wiley & Sons, Inc., Hoboken, NJ, USA, 2004.

[39] M.E.J. Newman. *Networks - an introduction*. Oxford University Press, New York, 2010.

[40] A.-L. Barabási and Z.N. Oltvai. Network biology: understanding the cell’s functional organization. *Nat. Rev. Gen.*, 5:101, 2004.

[41] T. Opsahl and P. Panzarasa. Clustering in weighted networks. *Social Networks*, 31:155–163, 2009.

[42] J.-P. Eckmann, E. Moses and D. Sergi. Entropy of dialogues creates coherent structures in e-mail traffic. *Proc. Natl. Acad. Sci. USA*, 101:14333–7, 2004.

[43] M. Faloutsos, P. Faloutsos and C. Faloutsos. On power-law relationships of the Internet topology. *Compute. Commun. Rev.*, 29:251–262, 1999.

[44] G. Caldarelli and M. Catanzaro. *Networks: A very short introduction*. Oxford University Press, New York, 2012.

[45] A.-L. Barabási, H. Jeong, E. Ravasz, Z. Néda, A. Schubert and T. Vicsek. *Physica A*, 311:590, 2002.

[46] A.-L. Barabási and R. Albert. Emergence of scaling in random networks. *Science*, 286:509–512, 1999.

[47] S. Allesina and S. Tang. Stability criteria for complex ecosystems. *Nature*, 483:205–208, 2012.

[48] W. Tarnowski, I. Neri and P. Vivo. Universal transient behavior in large dynamical systems on networks. *Phys. Rev. Research*, 2:023333, 2020.

[49] S. Sinha and S. Sinha. Evidence of universality for the May-Wigner stability theorem for random networks with local dynamics. *Phys. Rev. E*, 71(2):020902, 2005.

[50] M. Granovetter. Threshold models of collective behavior. *The American journal of Sociology*, 83:6, 1420–43, 2002.

[51] Y. Kuramoto. *Chemical oscillations, waves and turbulence*. Springer-Verlag Berlin, Heidelberg, 1984.

[52] P. Kundu, C. Hens, B. Barzel and P. Pal. Perfect synchronization in networks of phase-frustrated oscillators. *Europhysics Letters*, 120:40002, 2018.

[53] J.A. Almendral and A. Díaz-Guilera. Dynamical and spectral properties of complex networks. *New Journal of Physics*, 9:187–187, 2007.

- [54] P. Van Mieghem. Epidemic phase transition of the SIS type in network. *Europhysics Letters*, 97(4):48004, 2012.
- [55] P. Van Mieghem. *Graph Spectra for Complex Networks*. Cambridge University Press, Cambridge, UK, 2010.
- [56] V.S. Afraimovich and L.A. Bunimovich. Dynamical networks: interplay of topology, interactions and local dynamics. *Nonlinearity*, 20:1761–1771, 2007.
- [57] C. Kirst, M. Timme and D. Battaglia. Dynamic information routing in complex networks. *Nature Communications*, 7:11061, 2016.
- [58] A. Barrat, M. Barthélemy and A. Vespignani. *Dynamical Processes on Complex Networks*. Cambridge University Press, Cambridge, 2008.
- [59] G. Yan, G. Tsekernis, B. Barzel, J.-J. Slotine, Y.-Y. Liu and A.-L. Barabási. Spectrum of controlling and observing complex networks. *Nature Physics*, 11:779–786, 2015.
- [60] L. Schmetterer and K. Sigmund (Eds.). *Hans Hahn Gesammelte Abhandlungen Band 1/Hans Hahn Collected Works Volume 1*. Springer, Vienna, Austria, 1995.
- [61] S. Milojević. Power-law distributions in information science: making the case for logarithmic binning. *Journal of the American Society for Information Science and Technology*, 61:2417–2425, 2010.

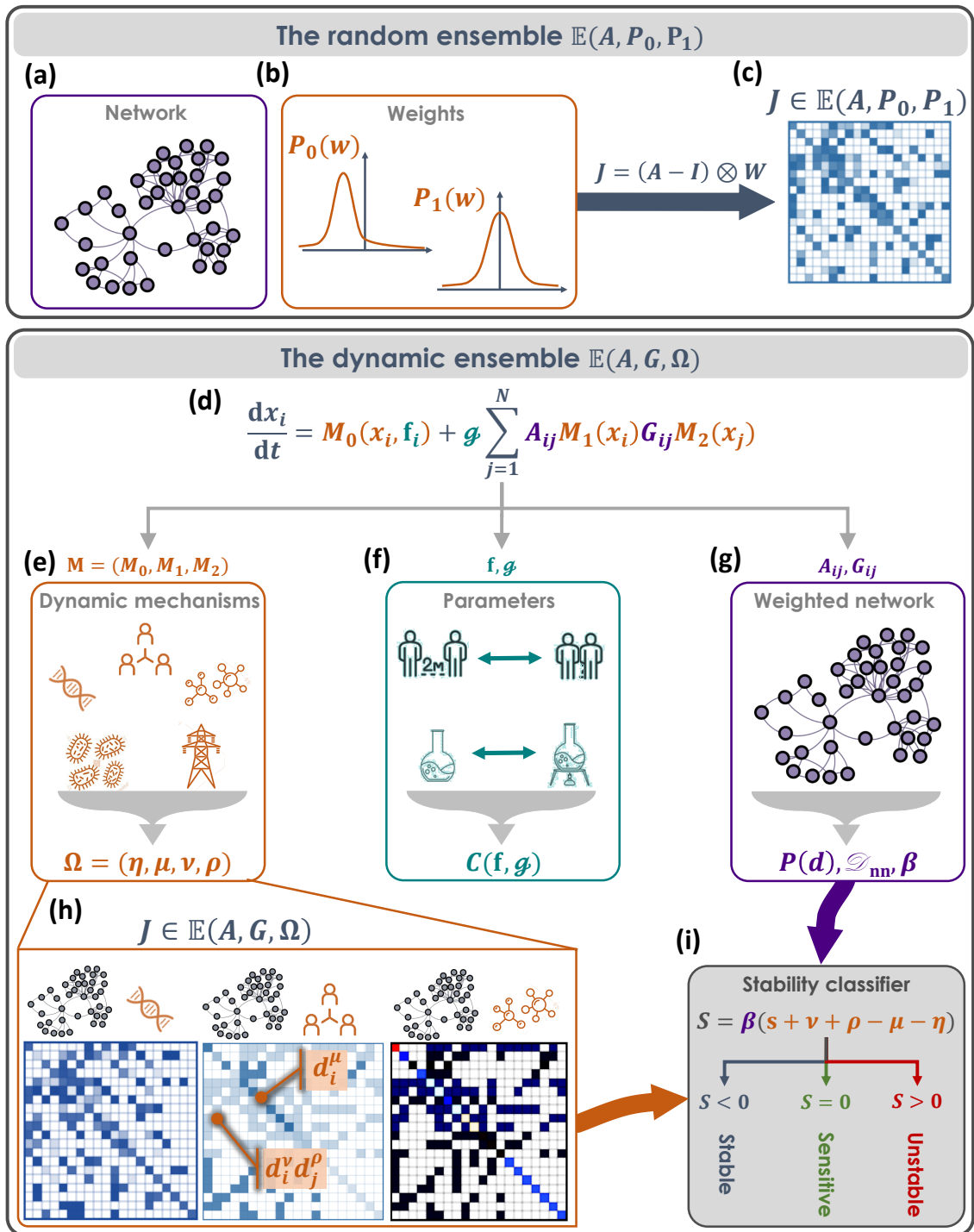
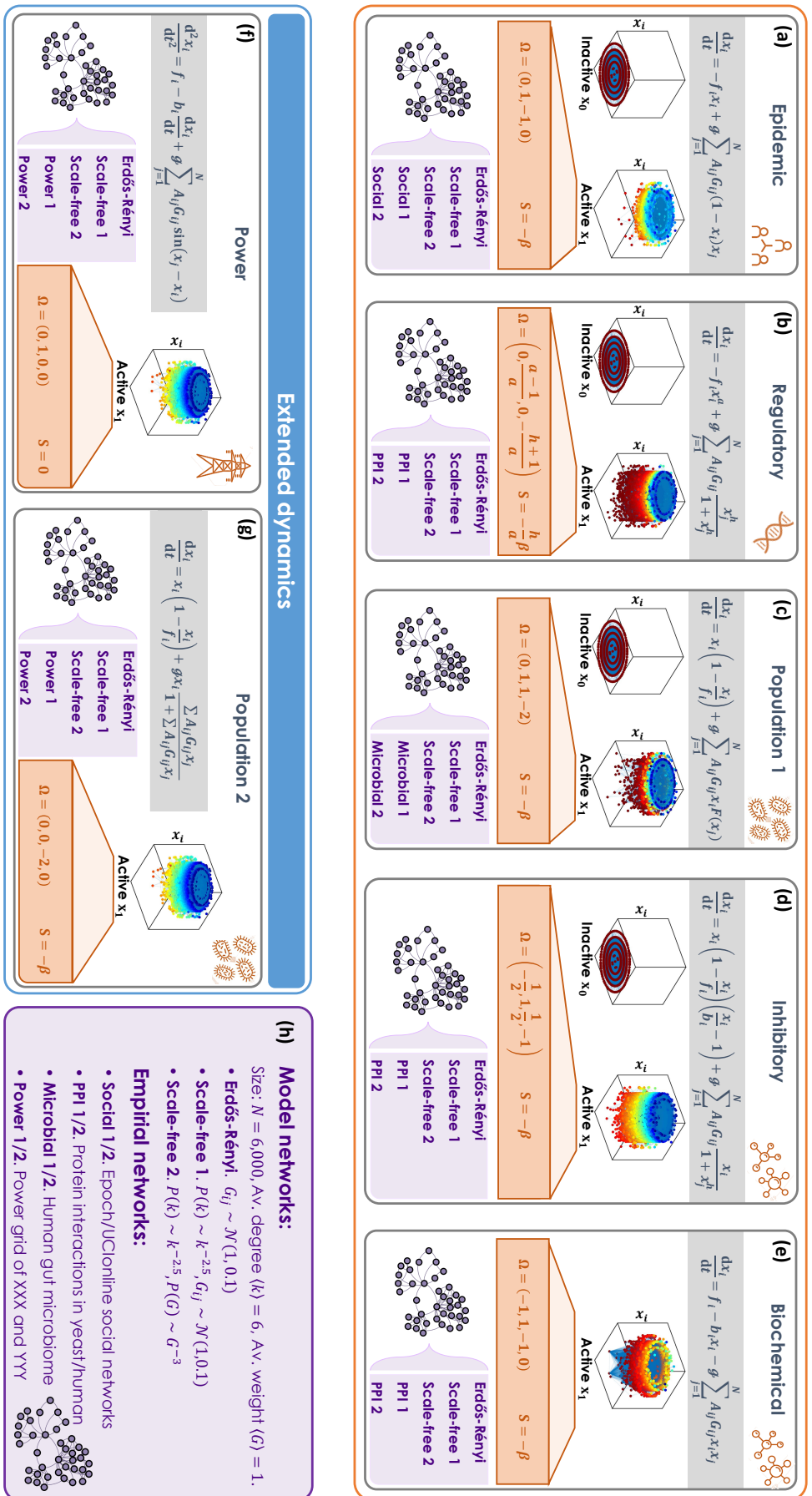
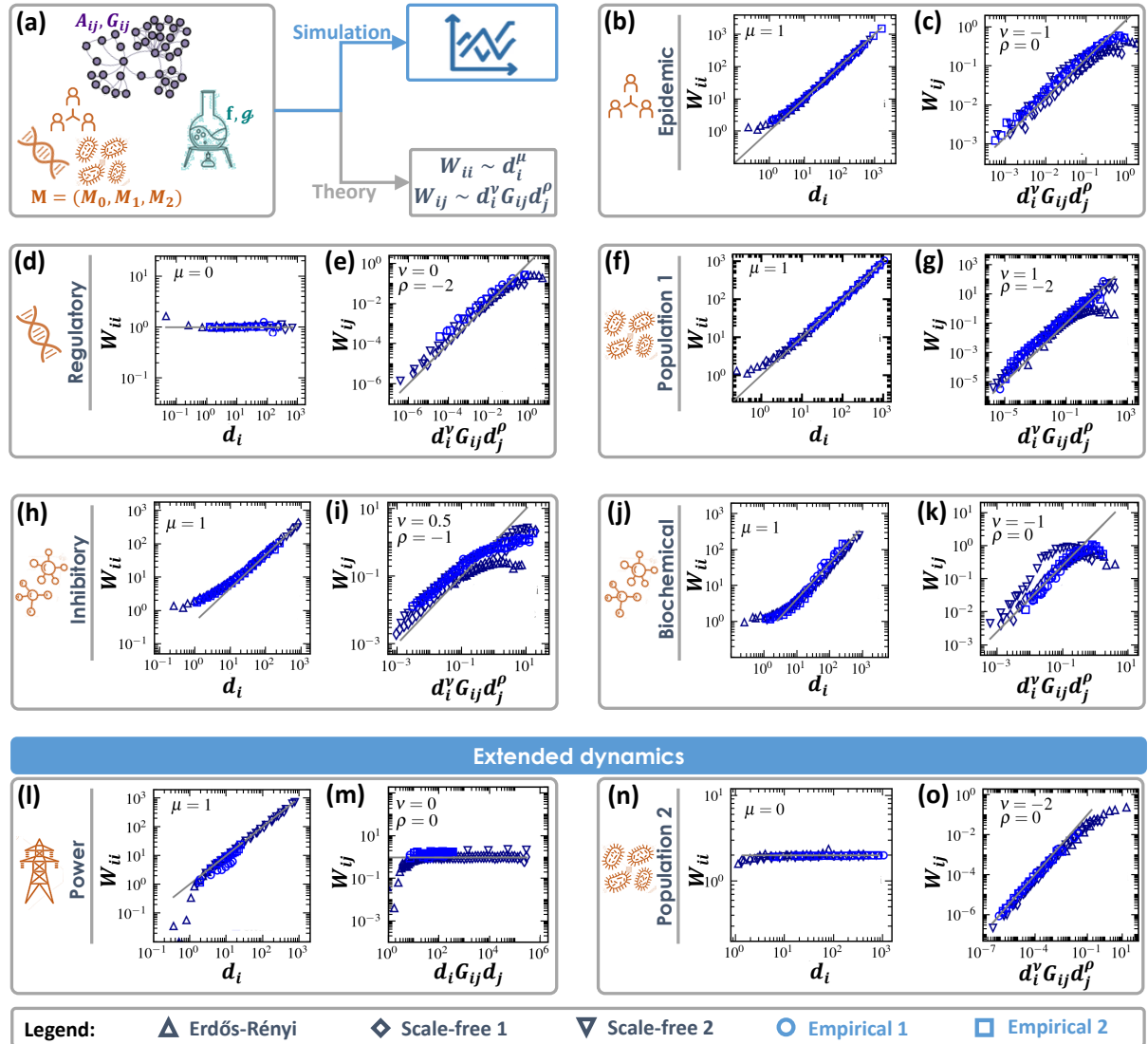


Figure 1 - full size. The dynamic Jacobian ensemble.

## Testing ground for $\mathbb{E}(A, G, \Omega)$





**Figure 3 - full size. Emergent patterns in the dynamic ensemble  $\mathbb{E}(A, G, \Omega)$ .**

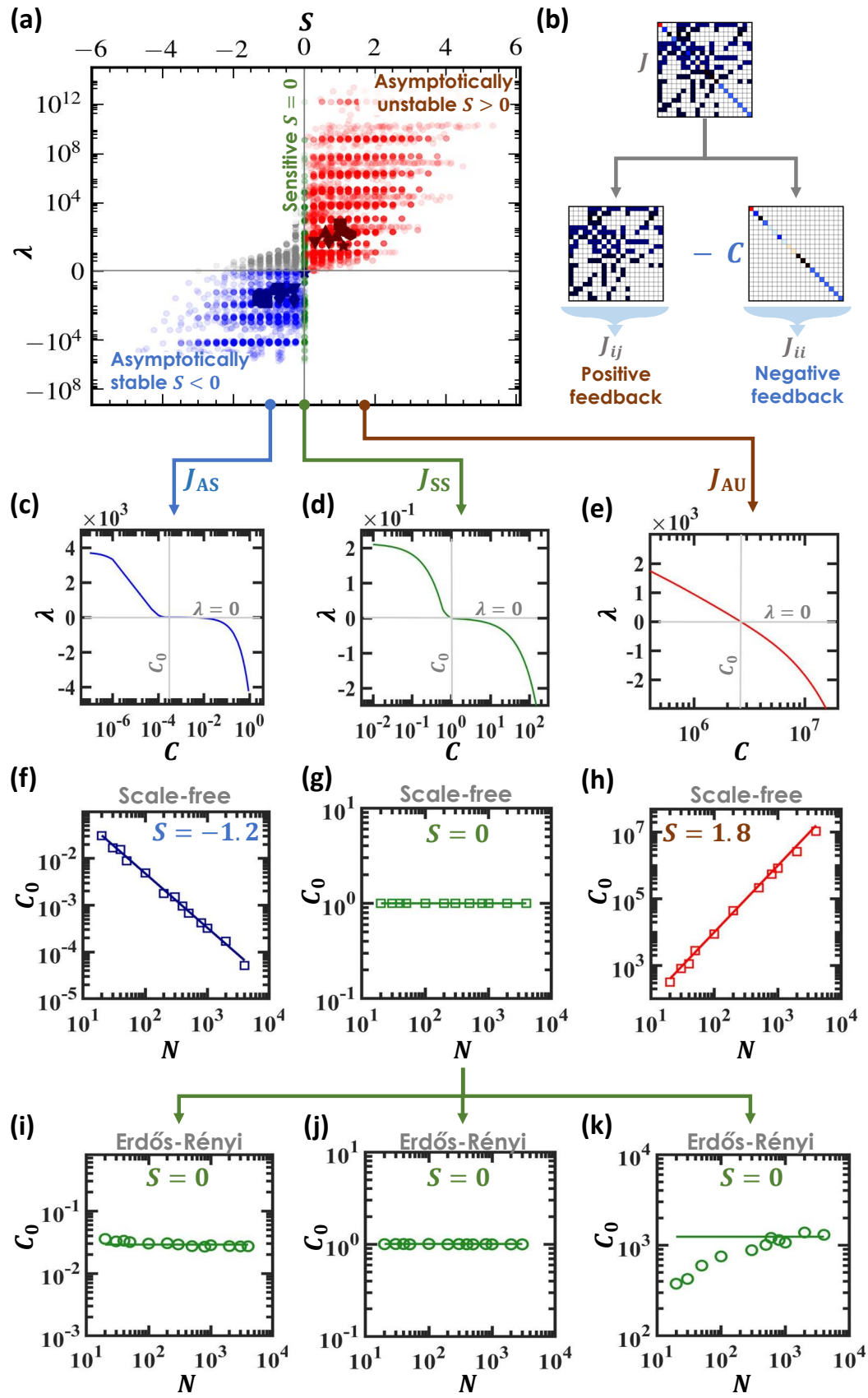


Figure 4 - full size. Three classes of dynamic stability in real and model networks.

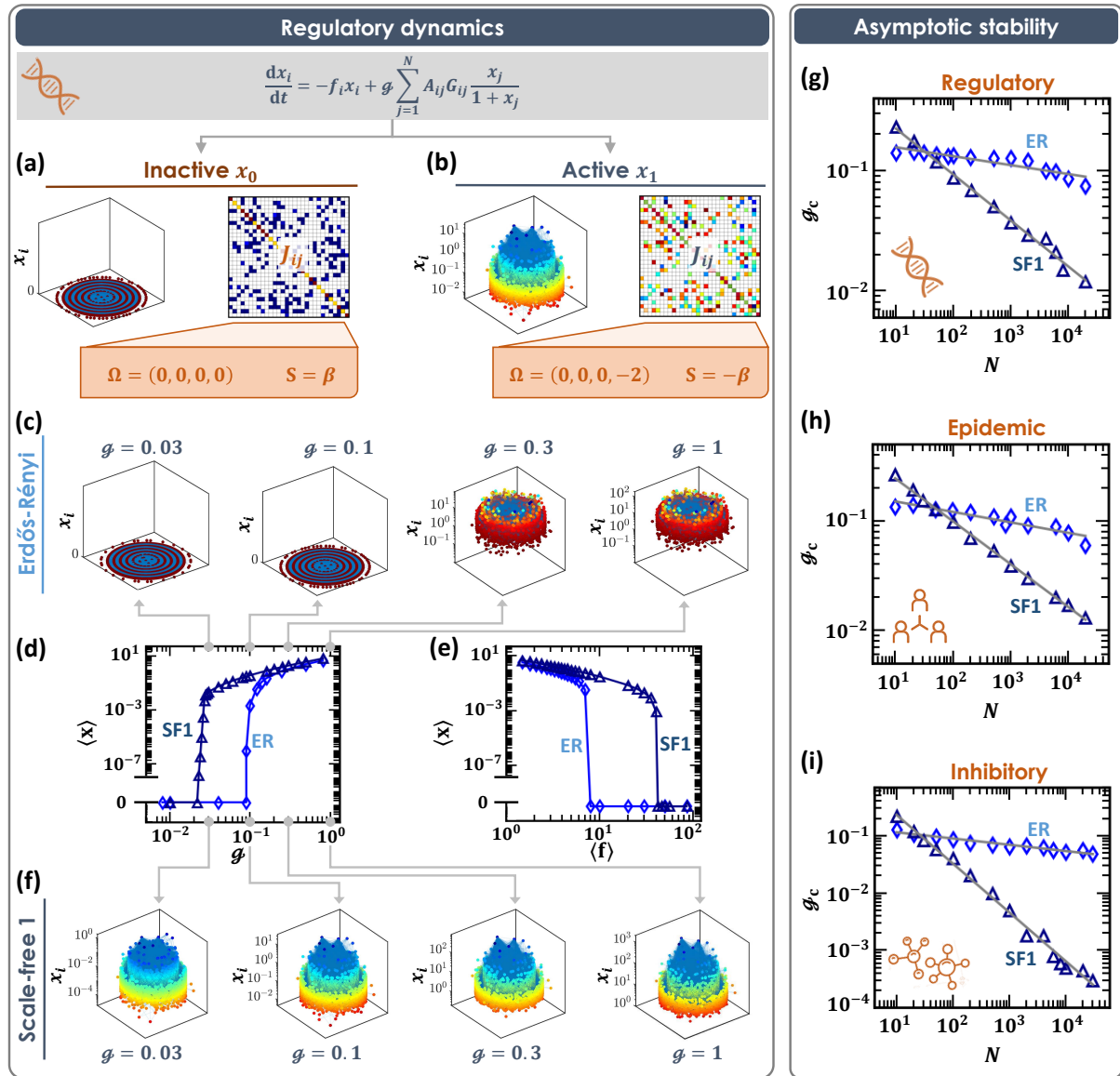


Figure 5 - full size. Emergent stability in large heterogeneous networks.

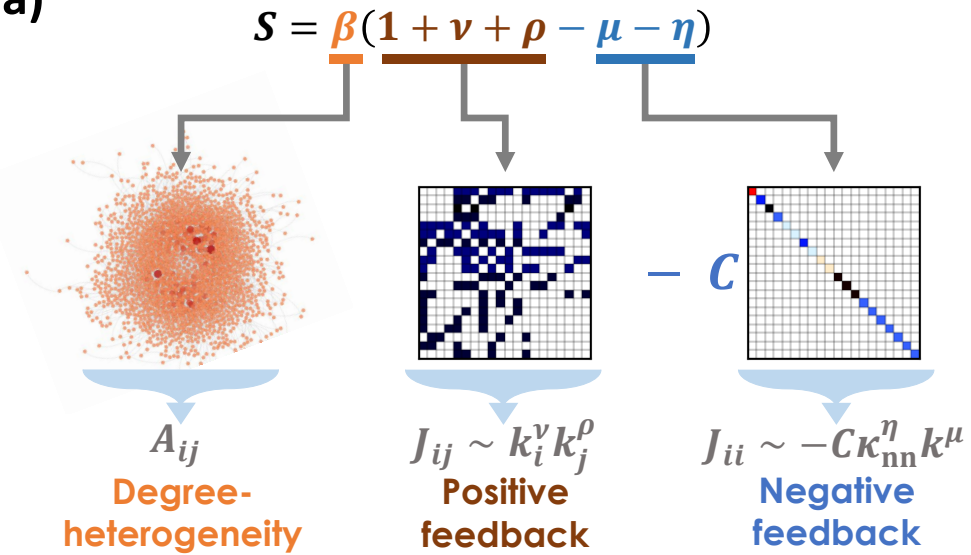
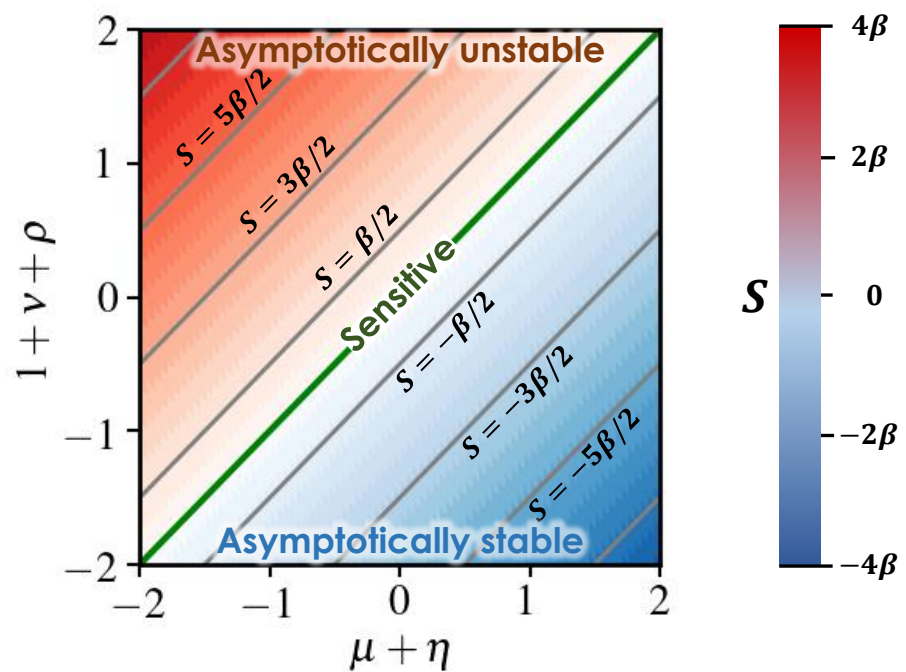
**(a)****(b)**

Figure 6 - full size. The ingredients of dynamic stability.